The Met Office operational wave forecasting system: the evolution of the Regional and Global models

Nieves G. Valiente[1], Andrew Saulter[1], Breogan Gomez[1], Christopher Bunney[1], Jian-Guo Li[1], Tamzin Palmer[1], Christine Pequignet[1]

5   [1]Met Office, Fitzroy Road, EX1 3PB, Exeter, UK

Correspondence to: Nieves G. Valiente (nieves.valiente@metoffice.gov.uk)

Abstract. The Met Office operational wave forecasting modelling system runs four times a day at the Met Office to provide global and regional forecasts up to 7 days ahead. The underpinning model uses a recent development branch of the 3rd generation spectral wave model WAVEWATCH III® (version 7.12) that includes several updates developed at the Met Office.

10 These include the Spherical Multiple-Cell (SMC) grid, rotated pole grid formulation for mid latitudes, enhancements to OASIS coupling and updates to the netCDF postprocessing. Here we document the technical details behind the system with a view to further developments. We focus on the global (GS512L4EUK) and regional (AMM15SL2) baseline configurations. GS512L4EUK is based on a multi-resolution four tier SMC 25-12-6-3km grid. The regional AMM15SL2 configuration covers the United Kingdom shelf using a two tier SMC 3-1.5km grid that also includes wave-current interactions. Evidence of

15 resolution dependent differences in wave growth were observed, leading to slightly overestimated significant wave heights in coastal mid-range conditions by AMM15SL2, but improved representation of extremes compared to GS512L4EUK. Additionally, although a positive impact of the surface currents is not always shown in the overall statistics of the significant wave height due to a larger spread in the observation-model differences, wave-current effects help to better capture the distribution of the energy in terms of frequency and direction near the coast (>20% improvement), which has implications to

20 beach safety, coastal overtopping risk and shoreline evolution. Future system developments such as the use of sea point wind forcing, the optimisation of the models in line with model resolution and the utilisation of SMC multigrid are discussed.

1 Introduction

Marine monitoring and prediction are crucial for the coastal and offshore sectors and having an accurate short range wave forecast is essential in many different applications. A wide range of areas such as marine navigation or offshore industries

25 (e.g., renewable energy offshore farms, fishing, commercial oil and gas extraction) rely on accurate forecasts to ensure a safe and timely functioning of their activities; and the forecasting of dangerous events that may lead to human and property risk is key for rapid decision making. Numerical weather prediction (NWP) models are used for operational weather and ocean forecasting, providing outputs to downstream users and forecasters. Met Office NWP systems for ocean forecasting include forecasts of ocean dynamics, waves, storm surges and ecosystems. These operational ocean forecasting models deliver

30 predictions of the marine environment contributing to safety at sea, industry and marine planning among others (Siddorn et al., 2016).

The National Centres for Environmental Prediction (NCEP) community spectral model WAVEWATCH III® (Tolman, 2014), herein WW3, is used operationally in both global and regional model configurations worldwide (e.g., GFSv16 wave (NOAA, 2020)). The Met Office runs an operational system of WW3 wave forecast configurations and research coupled atmosphere-wave-ocean models (e.g., Lewis et al., 2019; Bruciaferri et al., 2021; Castillo et al., 2022) that are based on a recent development branch of the community code (version 7.12). As part of the WW3 Development Group (WW3DG), the Met Office has contributed with several developments to the WW3 codebase, including:

- the Spherical Multiple-Cell (SMC) grid which provides an unstructured multi-resolution (i.e., coarser offshore with higher resolution in coastal waters) spatial grid (Li, 2012) to improve model efficiency and enable improved forecast skill toward coastal zones;
- rotated pole grid formulation for mid latitudes;
- enhancements to the OASIS coupling for compatibility with ocean and atmospheric models;
- and updates to the netCDF postprocessing. These include grid interpolation from SMC to regular grids for products generation, CF compliant netCDF and user configurable netCDF metadata to maintain consistency with Copernicus Marine service naming conventions.

This paper documents the deployment of these recent WW3 developments in the Met Office operational wave forecasting systems. Particular attention is paid to the impact of resolution and the effect of wave-current interactions on model accuracy. A description of the operational wave modelling system with focus on the global and regional UK waters baseline configurations is presented in Sect. 2. Methods and data sources for evaluating model performance are presented in Sect. 3. The operational forecast skill of the system is shown in Sect. 4 and an additional assessment of the accuracy of the models with a view to further development is described in Sect. 5. Finally, a discussion with key challenges and future work and conclusion are presented in Sect. 6 and 7, respectively.

2 The Met Office operational wave models

The Met Office operational forecasting system (Table 1) includes a global deterministic configuration (GS512L4EUK), and two regional configurations, a deterministic nested one-way covering the Northwest (NW) European shelf and UK waters (AMM15SL2), and an Atlantic wave ensemble (AS512L4EUK) (Fig. 1). AMM15SL2 is run both as a standalone wave model (i.e. forced one-way by winds and surface currents) and as the wave component of the FOAM-AMM15 ocean-wave coupled operational system (AMM15 coupled; e.g., Lewis et al., 2019) used to produce Copernicus Marine Service products (Saulter, 2020b) from the Northwest Shelf Monitoring and Forecast Centre (NWS-MFC; e.g.: https://marine.copernicus.eu/about/producers/nws-mfc). This section describes the model and baseline configurations GS512L4EUK and AMM15SL2. For additional information on AS512L4EUK and AMM15 coupled models refer to Bunney and Saulter (2016), and Tonani et al. (2019) and Bruciaferri et al. (2021), respectively.
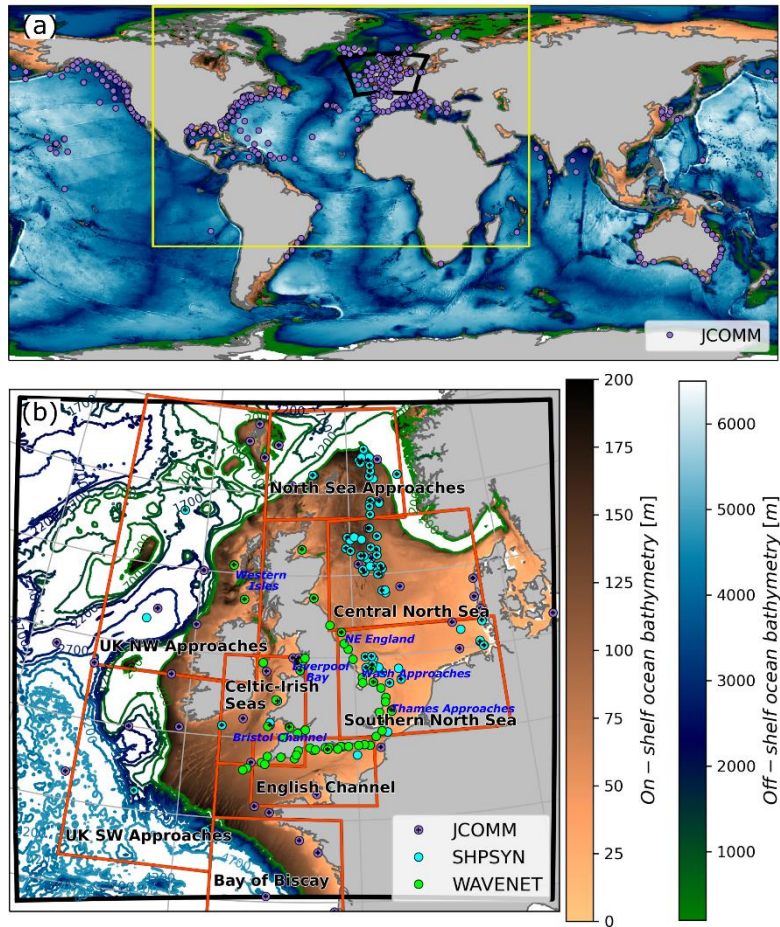
Figure 1. (a) Global and **(b)** northwest (NW) European shelf – UK waters physical context and model domains. Yellow box and black solid line in **(a)** indicate the cut-off area for the Atlantic wave ensemble and the NW European shelf – UK waters domains, respectively. **(b)** NW European shelf – UK waters domain with areas used for analysis indicated in red. In-situ observations are shown as solid dots. In-situ observations include the Joint WMO IOC Commission for Oceanography and Marine Meteorology's operational Wave Forecast Verification Scheme (JCOMM), Ship Synop Ob-servations at fixed platforms (SHPSYN) and UK WAVENET and National Network of Regional Coastal Monitoring Programmes in-situ observations for coastal waters (WAVENET). Locations where there is overlap with JCOMM observations are marked with a cross.

2.1 Model description

The Met Office operational wave forecasting system is based on the WAVEWATCH III® third-generation spectral model (Tolman, 2014) at version 7.12. This model resolves the evolution of the phase-averaged two-dimensional (frequency-direction) wave energy spectrum in time and space using the net effect of sources and sinks of wave energy; i.e., a total source term describing local wave energy growth and dissipation, and advection of wave energy through the wave model grid. To enable conservation in the presence of ocean currents, the model describes these changes in terms of wave action (Ardhuin et al., 2012, 2017). The total source term is defined by the combination of different physical processes that, in deep waters, can be simplified to a wind-wave interaction term that describes transfer of momentum from the atmosphere to the ocean surface

waves, a nonlinear wave-wave interaction term that describes energy transfers between waves of different frequencies, and a dissipation term describing loss of energy from the waves to the surrounding ocean and atmosphere (Valiente et al., 2021a). Additionally, the operational systems include a linear input term used to initialise wave growth and parameterizations of shallow water processes (i.e., depth-induced breaking and wave bottom interactions). The total source term is therefore defined as:

$$S_{total} = S_{in} + S_{nl} + S_{diss} + S_{bf} + S_{brk}$$

WW3 provides multiple options for both source term parameterizations and numerical advection (WW3DG, 2019). This section summarizes the options chosen for the Met Office operational configurations. More details of the compilation switches and source term tuning values can be found in the *Supplementary Material.*

The Met Office operational wave forecasting systems use the Ardhuin et al. (2010) ST4 package to parameterise wave growth (S_{in}) and dissipation via whitecapping (S_{diss}). The family of parameterisations in ST4 defines S_{in} based on WAM cycle 4 parameterisation (Janssen, 2004) with an ad-hoc reduction of the wind contribution to account for the impact of long waves on short waves through a tuneable sheltering coefficient (TAUWSHELTER=0.3; refer to Table S2 in *Supplementary material*) that decreases the drag coefficient at high winds (Saulter et al., 2017; Valiente et al., 2021a). For compatibility with Met Office Global Unified Model wind forecast data, a minor adjustment on the control of the input wind stress (BETAMAX namelist value set to 1.39; refer to Table S2 in *Supplementary material*) has been implemented across both global and regional wave models. The BETAMAX value is also adjusted for the case of the ocean-wave regional coupled configuration which is forced by ECMWF winds (BETAMAX namelist value of 1.48; refer to Table S2 in *Supplementary material*). Input wind stress to S_{in} is derived using conversion from atmospheric model 10m neutral wind speed to momentum stress flux computations which are included in the source term (FLX0); i.e., stress is defined implicitly inside the source terms subroutines. The model assumes neutral atmospheric stability in these calculations. Additionally, a switch with linear wave growth (LN1; Cavaleri and Rizzoli, 1981) for lower winds is implemented (Valiente et al., 2021b), to enable the consistent spin-up of the model from calm conditions and a more accurate description of the initial wave growth.

S_{diss} is parameterised from the wave spectrum saturation following the ideas of Phillips (1985) with the integrations over directions presented in Ardhuin et al. (2010). The Discrete Interaction Approximation (DIA) package (NL1; Hasselmann et al., 1985) is used to resolve (S_{nl}) nonlinear wave–wave quadruplets interactions that enable downshifting of energy input in the upper tail of the wave spectrum into longer waves. NL1 is developed for deep water, using the appropriate dispersion relation for resonant wave interactions. For shallow water, this source term uses a scaled version of the deep-water dispersion relation. As part of the shallow water physics, the Met Office wave model configurations include source terms to resolve depth induced refraction, shoaling and breaking. Shallow water wave energy dissipation includes the surf breaking parameterisation proposed by Battjes and Janssen (1978) (DB1) and JONSWAP bottom friction formulation (BT1; Hasselmann et al., 1973). Model spectral resolution is identical in all the wave operational systems with 30 frequencies logarithmically spaced between 25 to 1.5 seconds (starting at 0.04118Hz) and 36 directional bins that are linearly spaced.

Advection of wave energy through the model grid satisfies the wave dispersion relationship, for which wave energy at lower frequencies will travel more rapidly through the model grid than waves at high frequencies. All configurations of the Met Office operational forecasting system utilise the SMC grid (Li, 2012). One of the key features of this grid is that it allows higher resolution cells in areas of interest (shallow water, coastal areas and islands) whilst maintaining coarse resolution in the open ocean for computational efficiency. The SMC grid retains the quadrilateral cells as in the standard latitude-longitude grid so that simple finite difference schemes could be used. Sub-time-steps are applied on different cell sizes to speed up propagation calculations with a choice of 2nd or 3rd order upstream non-oscillatory (UNO) advection schemes (Li, 2008). The refraction induced wave spectral rotation and the great circle turning are combined and calculated with a re-mapping scheme, which is not subject to the Courant–Friedrichs–Lewy (CFL) restriction but to a physical limit not exceeding the bathymetry gradient direction or a user defined limit angle. Grid cells are merged at high latitudes to relax the CFL restriction and a fixed reference direction is used to define wave spectra in the polar region so that the whole Arctic Ocean could be included in the global domain. The multi-resolution refinement is useful to resolve small islands and coastline details, which are important in ocean surface wave propagations (Saulter et al., 2017). The *Garden Sprinkler Effect* (GSE) caused by the discrete directional bins of the wave energy spectrum is alleviated with a diffusion term similar to the PR2 option in WW3 model (Booij and Holthuijsen, 1987), plus an optional averaging scheme for further smoothing (WW3DG, 2019).

Table 1 Specifications of the operational production of all the Met Office wave models: GS512L4EUK, AS512L4EUK, AMM15SL2 and AMM15 coupled.

		Forecast Run	Update Run
GS512L4EUK	*Forecast length and run frequency*	T+144 for 0ZZ, 12Z T+66 for 6Z, 18ZZ	T+6 for 0Z, 6Z, 12Z, 18Z
	Wind forcing	Hourly NWP global forecast at 10km resolution	Hourly NWP global update at 10km resolution
	Ice forcing	Global OSTIA at 1/12º resolution	Global OSTIA at 1/12º resolution
	Initialisation	Restart file update T+6	Restart file update T+6
	Boundary conditions	--	--
AS512L4EUK	*Forecast length*	T+168	--
	Run frequency and members	00Z/12Z:0-17 members, 06Z/18Z:0,18-34 members	--
	Wind forcing	Hourly NWP MOGREPS-Global forecast atmospheric ensemble at 20km resolution	--
	Ice forcing	Global OSTIA at 1/12º resolution	--
	Initialisation	Restart file update T+6	--
	Boundary conditions	2D spectral boundary conditions at 25 km resolution	--
AMM15SL2	*Forecast length and run frequency*	T+66 for 0Z, 06Z, 12Z, 18Z	T+6 for 0Z, 6Z, 12Z, 18Z
	Wind forcing	Hourly NWP global forecast at 10km resolution	Hourly NWP global update at 10km resolution
	Current forcing	Hourly AMM15 (00Z) at 1.5km resolution	Hourly AMM15 (00Z) at 1.5km resolution
	Initialisation	Restart file update T+6	Restart file update T+6
	Boundary conditions	2D spectral boundary conditions at 25 km resolution	2D spectral boundary conditions at 25 km resolution
AMM15 coupled	*Forecast length*	T+144	--
	Run frequency	00Z	--
	Wind forcing	Hourly ECMWF forecast winds for T0 to T72 3-hourly ECMWF forecast winds for T72 to T144	--
	Initialisation	T-48 hindcast cycle. Restart file T-24	--
	Boundary conditions	2D spectral boundary conditions at 25 km resolution	--
	Hindcast	T-48 using hourly ECMWF winds from previous analysis cycle	--

2.2 Baseline configurations of the operational forecasting system

2.2.1 GS512L4EUK Global

The wave forecast global model configuration GS512L4EUK covers the globe from 80° S to 86° N (Fig. 1a) using model bathymetry based on GEBCO 2014. The model grid is a four-tier SMC 25-12-6-3km refined grid, for which the coarsest cells are located in open waters and resolved at approximately 25km (0.35° longitude by 0.23° latitude) in mid-latitudes. The 25-km cells represent a base resolution equivalent to an N512 atmosphere model and are successively halved to 12km, 6km and 3km as the grid gets closer to the coastline. An area of special interest is designated in UK waters, where higher resolutions are applied more widely (Saulter et al., 2016). The Atlantic ensemble forecast system for prediction of Atlantic-UK wind

waves (AS512L4EUK; Bunney and Saulter, 2015; Saulter et al., 2016) is based on a cropped version of the GS512L4EUK grid from 25° S to 83° N. Refer to Bunney and Saulter (2015) for a detailed information on the ensemble model.
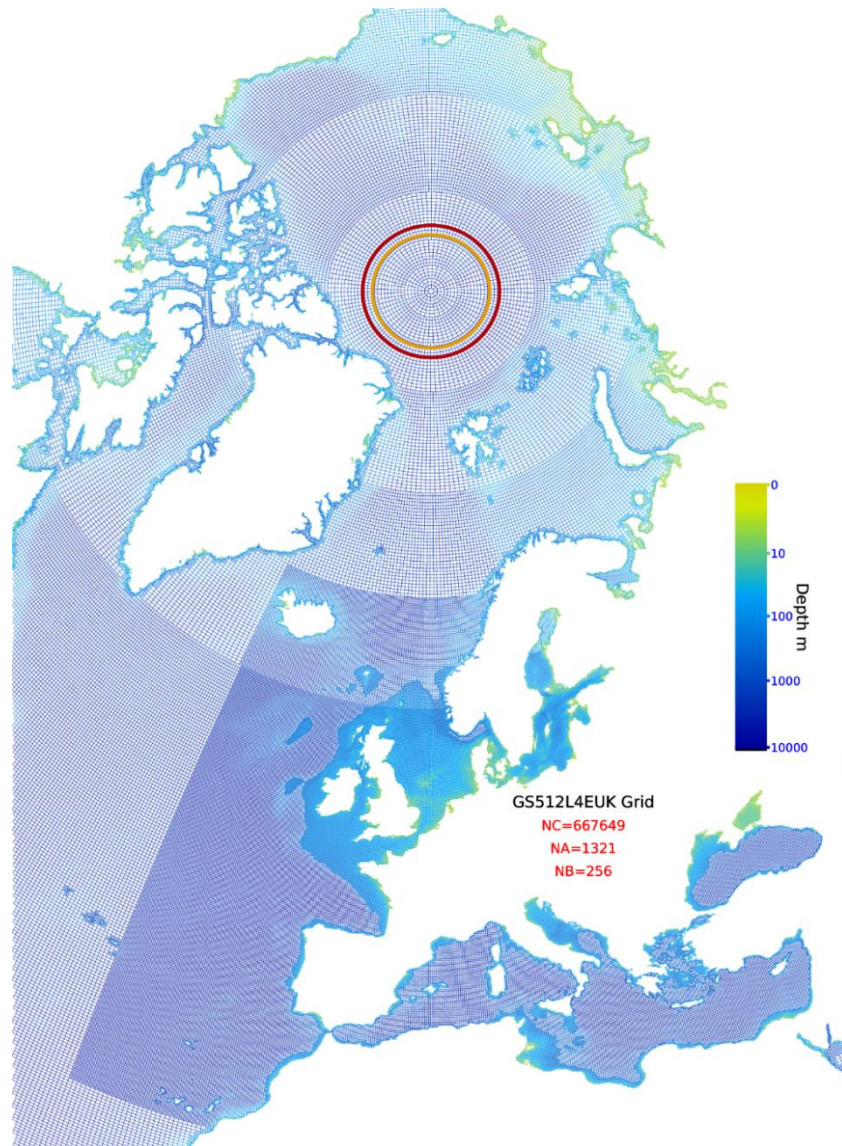
140

Figure 2. Spherical Multiple-Cell (SMC) GS512L4EUK global model grid across the European-Arctic region. Coarsest (open waters) cells are resolved at approximately 25km in mid-latitudes (0.35° longitude by 0.23° latitude) and reduced by a factor of two to 12km, 6km and 3km. 12km cell size are set over the European region (27N 25W to 68N 42E) with a reduction to 6km for cells with depths less than 320m depth and to 3km for those cells around the UK coastline.

145   Fig. 2 shows the European-Arctic region of the GS512L4EUK global model grid. Over an Europe-wide region (covering approximately 25° W to 27° E and 42° N to 68° N), the coarsest cell size has been set to 12km so that the model can exploit the full detail of the current Met Office global atmosphere-ocean model (approximately 10km resolution), whilst any cells with

depths less than 320m are resolved at 6km. This depth was chosen as a threshold to apply higher resolution since wave energy with mean periods of about 18s or longer will begin to interact with the seabed. The use of the 3km cell refinement is restricted

150 to coastal cells on the NW European shelf (45° N 16° W to 61.15° N 9.4° E) to best represent the coastline of the UK (Saulter et al., 2016) whilst minimising computational costs. At higher latitudes, longitudinal cell sizes are doubled (by a factor of two at 60° N, four at 75° N, eight at 83° N) in order to support a larger CFL time-step than would be permitted by a regular latitude-longitude grid (Li and Saulter, 2014; Saulter et al., 2016). The Arctic part (cells inside golden circle in Fig. 2) is not used in the operational forecast system at present since for most of the time it is covered by sea ice.

155 The GS512L4EUK model is forced by hourly global atmospheric 10m neutral wind files and ice concentration interpolated to the coarsest resolution of the SMC grid (i.e., 25km). 10m neutral winds are provided by a high-resolution atmosphere-ocean coupled global configuration (Williams et al., 2018) of the Unified Model (UM; e.g., Walters et al., 2019; Brown et al., 2012) and NEMO ocean model each hour; the atmosphere-ocean coupled model has 0.23° longitude by 0.16° latitude resolution (N1280L70; 2560 latitude x1920 longitude and vertical 70 levels), with approximately 10km grid length in mid latitudes. Ice

160 concentration is provided by the Operational Sea Surface Temperature and Sea Ice Analysis (global OSTIA; Good et al., 2020) also produced at the Met Office. GS512L4EUK uses simple ice blocking (IC0) where grid points covered by ice are treated as land and a cut-off ice concentration value of 50% at which obstruction is used. This global model provides full 2D spectral boundary conditions for the nested operational wave (AS512L4EUK, AMM15SL2-UK waters) and AMM15 ocean-wave coupled configurations.

165 **2.2.2 AMM15SL2 NW shelf-UK Waters**

AMM15SL2 covers the NW shelf-UK area from approximately 45° N 20° W to 63° N 12° E with a resolution of 3-1.5km. The domain extends beyond the shelf break in order to take boundary conditions in open waters which are not subject to shallow water processes, but is primarily focused on forecasting the shelf seas around the UK; i.e., Celtic and Irish Seas, North Sea, and English Channel (Fig. 1b). The AMM15SL2 configuration name is derived from the AMM15 (1.5km NW Shelf

170 Atlantic Margin Model) ocean model that encompasses the same region and the use of a two-level SMC grid refinement (Li, 2011) with variable resolution based on both proximity to coast and water depth (Saulter et al., 2017; Valiente et al., 2021b). The grid resolution is of 3km for water depths larger than 40m and 1.5km for coastal cells with water depths of less than 40m (Fig. 2). The SMC grid is based on a rotated north pole at 177.5° E 37.5° N, achieving an evenly spaced mesh around UK. Bathymetry and coastal masking for this configuration are the same as the 1.5km AMM15 NEMO (Nucleus for European

175 Modeling of the Ocean; Madec, 2008) based ocean configuration (Tonani et al., 2019; Graham et al., 2018). Bathymetry and land-sea mask are based on the European Marine Observation and Data Network (EMODnet portal, September 2015 release) corrected to mean sea level (Tonani et al., 2019).

AMM15SL2 is the baseline configuration used for the UK waters wave-only and AMM15 ocean-wave coupled models. AMM15SL2 wave-only is driven by hourly NWP 10m neutral winds from the global UM-NEMO operational system and is

180 also forced by hourly currents from the regional AMM15 Ocean-Wave Coupled Model shelf seas Forecast Ocean Assimilation

Model (AMM15-FOAM; Tonani et al., 2019, see next Sect. for a summary of details) interpolated in time and space to the underlying 3km cell resolution regular grid version of the SMC. The coupled version of this configuration differs from the AMM15SL2 UK waters wave model in the forcing sources, being driven by surface (10m) wind data at approximately 9km resolution provided from the atmospheric high-resolution global configuration of the Integrated Forecast System run at the European Centre for Medium-Range Weather Forecasts (ECMWF; https://www.ecmwf.int/en/forecasts/documentation-and-support). The wave model is two-way coupled to the ocean NEMO model AMM15-FOAM using the Ocean Atmosphere Sea Ice Soil (OASIS-MCT coupler; Valckle et al., 2015) coupling libraries. The coupling configuration passes atmosphere to ocean stress, calculated by the wave model, from wave-to-ocean, and surface currents from ocean-to-wave. The ocean component integrates a NEMO physical ocean model and the Nucleus for European Modelling of the Ocean data assimilation system (NEMOVAR; e.g., King et al., 2018; Waters et al., 2015). NEMOVAR uses a 3D-Var first guess at appropriate time (FGAT) scheme which includes bias corrections scheme for both sea surface temperature and altimeter data.

2.3 Operational production

Operationally, GS512L4EUK and AMM15SL2 wave models run four cycles per day (00Z, 06Z, 12Z and 18Z; Table 1) to T+66. The 00Z and 12Z cycle on each day are extended to a 144hour forecast for GS512L4EUK. Both GS512L4EUK and AMM15SL2 are initialised using the restart file T+6 from a short 6hour "update cycle" using the most up-to-date NWP winds. This way all models provide a forecast that it is initialised with the best available descriptions for atmosphere and ocean (i.e., with as many observations assimilated as possible). Ice concentration from global OSTIA for GS512L4EUK, and currents from AMM15-FOAM for AMM15SL2 are updated once a day at 00Z. The AMM15SL2 wave at 00Z runs before the ocean-wave coupled AMM15 00Z in the Met Office production cycle, forcing this cycle to use the forecasted currents from the previous day's AMM15 ocean-wave model cycle (i.e., currents at T+24 from previous cycle of AMM15 coupled). The AMM15 ocean-wave coupled model runs once a day triggering a 144hour forecast. Each model cycle starts with a T-48 hours hindcast prior to each forecast. Refer to Saulter (2020a) and Tonani et al. (2021) for more information on the production cycle of CMEMS AMM15 ocean-wave coupled.

AS512L4EUK wave ensemble currently runs as a "lagged" ensemble: members 0 to 17 run to full length (168hour) at 00Z and 12Z whereas members 0 and 18 to 34 run at 06Z and 18Z. A full 36 member lagged ensemble is made up at each cycle from overlapping full length members.

3 Observations and metrics for model accuracy

Modelled waves and winds are evaluated using significant wave height (H_s), mean zero up-crossing period (T_{02}) and mean wave direction (Dir) for the waves, and 10m height wind speeds (U_{10}) and wind direction (U_{10} dir) for the wind forcing conditions. These parameters are widely used for model evaluation as they give information concerning the wave model

performance in aspects such as bulk energy imparted to the ocean surface waves and representation of the wave energy distribution through the frequency domain and directional space (Saulter A., 2020b).

Wave parameters from the model simulations are assessed using four different datasets: (i) 6/12-hourly in-situ data from the Joint WMO-IOC Commission for Oceanography and Marine Meteorology's operational Wave Forecast Verification Scheme (Bidlot et al., 2007), hereafter JCOMM-WFVS, for H_s and T_{02}; (ii) hourly Daily Ship Synoptic Observations at fixed platforms for H_s and T_{02} across the NW shelf, hereafter SHPSYN; (iii) hourly UK WAVENET and National Network of Regional Coastal Monitoring Programmes (NNRCMP) in-situ observations for coastal waters comprising Waverider buoy measuring H_s, T_{02} and Dir, hereafter WAVENET; and (iv) global satellite merged altimeter data (hereafter MA_SUP03) including JASON 2, CryoSat and SARAL AltiKa H_s data. Wind forcing conditions (U_{10} and U_{10} dir) are verified using JCOMM-WFVS, SHPSYN and MA_SUP03 datasets.

Basic metrics for model evaluation are described in *Supplementary material*. These include *bias*, root mean square deviation (*RMSD*), observations (*SDobs*) and model standard deviation (*Sdmodel*), Pearson correlation coefficient (*r Pierson*), standard deviation of the error (*StdE*), covariance (*Cov*), and variance (*Var*). Extreme verification and extra metrics for model evaluation are also provided and include Scatter Index (*SI*) and Symmetric Slope (*SS*) between the model and the observations. *SI* is calculated dividing the standard deviation of model-observation differences and *Sdobs*. The *SS* is described as the ratio of model variance to observations variance. *Bias* and *RMSD* are used to document the forecast accuracy whereas all the metrics are presented for the model evaluation.

4 Forecast performance

The quality of the Met Office short range forecasting system is evaluated by running and verifying the two baseline global (GS512L4EUK) and regional (AMM15SL2) UK waters (refer to Fig. 1a,b) configurations during 50 days in summer (from 20190619 to 20190814; JJA) and winter (20191204 to 20200124; DJ). These experiments (Table 2) replicate the operational configurations described in *Sect. 2.2*. Initial conditions for FCST experiments used the corresponding T+6 restart output file generated during the analysis experiments (previously run). For comparison purposes, AMM15SL2-FCST was run up to T+144 as per GS512L4EUK-FCST, as opposed to T+66 used in operations. It is noted that currents used as forcing were not available in the last 78 hours of the AMM15SL2-FCST runs.

Table 2 Experiments specifications for forecast capability.

Experiment	Description
GS512L4EUK-FCST	JJA (20190619 to 20190814) and DJ (20191204 to 20200124) forecast run global. Forcing: forecast 10km hourly NWP winds and updated fraction of sea ice. Restart at T+6 T+144 forecast at 00Z cycle
AMM15SL2-FCST	JJA (20190619 to 20190814) and DJ (20191204 to 20200124) forecast. Forcing: forecast 10km hourly NWP winds and AMM15 FOAM analysis and forecast hourly currents. Restart at T+6 T+144 forecast at 00Z cycle

Forecast skill, from T+24 hours to T+144 hours, of wind and wave parameters across the NW shelf area over the summer months of JJA and the winter months of DJ for the two baseline configurations is presented in Fig. 3. Winds tend to be
240 overestimated in both configurations during most of the forecasting period up to T+96 (GS512SL4EUK and AMM15SL2 *biases* are 0.4–0.6 and 0.1–0.3ms^{-1}, respectively; Fig. 3a). At longer forecast lead times, winds appear to be slower versus the first forecast days, and the tendency is to show a reduced *bias* that might be also associated with compensating errors (*biases*=0.1 and -0.2 ms^{-1} for GS512SL4EUK and AMM15SL2 at T+144). This is also observed in H_s biases where values are also slightly overestimated (*biases*=0.1 and 0.2m for GS512SL4EUK and AMM15SL2) and model-observation differences
245 are smaller during the winter months (0.02 and 0.1m for GS512SL4EUK and AMM15SL2, respectively; Fig. 3c).

Despite the bias reduction observed in U_{10} and H_s, the forecast skill of both configurations decreases with lead time (i.e., positive trend) and is slightly weaker during the winter months for both forcing and wave bulk parameters (i.e., U_{10}, U_{10} dir, H_s and T_{02}), suggesting a consistent behaviour across model resolution. The decrease in the forecast skill appears to be relatively steady for the first four days of forecast (U_{10} *RMSD*=1.5–2.5ms^{-1} and H_s=0.1-0.4m up to T+96 in JJA; Fig. 3b,d);
250 however, *RMSD* trend indicates a more rapid decrease in the forecast skill after these (increases to 3.5ms^{-1} and 0.6m at T+144). It is noted that the degree of decrease in the forecast skill for the case of T_{02} is smaller compared with H_s and, in fact, values of both *bias* (-0.8s and -0.5s for GS512SL4EUK-FCST and AMM15SL2-FCST, respectively; Fig. 3g) and *RMSD* (1.4s and 1.1s for GS512SL4EUK-FCST and AMM15SL2-FCST, respectively; Fig. 3h) are almost constant for the first four days in both JJA and DJ (Fig. 3g,h) periods.
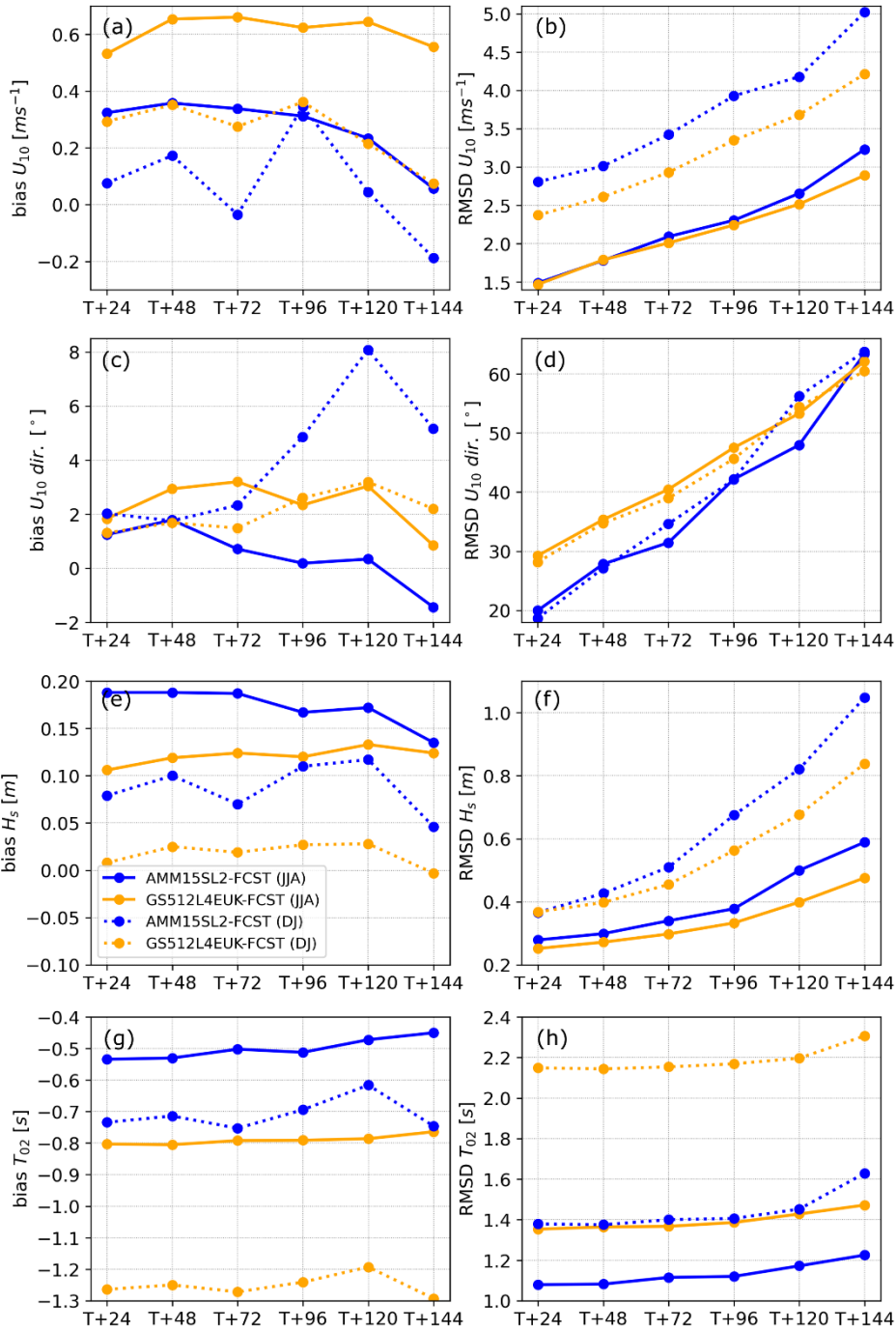
255

Figure 3. Forecast (a,c,e,g) *bias* and (b,d,f,h) root mean square deviation (*RMSD*) for wind speed (U$_{10}$; a,b), wind direction (U$_{10}$ dir; c,d), significant wave height (H$_s$; e,f) and mean period (T$_{02}$; g,h) every 24 hours over a forecast period of 6 days (T+144) for the area of the NW shelf. Values are averaged over the months June-July-August (JJA; solid lines) and December-January (DJ; dotted lines) and correspond to the NW shelf – UK waters model (AMM15SL2-FCST; blue) and the global model (GS512L4EUK-FCST; orange).

260 Model forecast skill for H_s suggests that the positive impact of including the surface currents and having increased resolution is not always shown in the overall statistics. Indeed, H_s *bias* and *RMSD* for the regional baseline configuration during the forecast period are greater (AMM15SL2-FCST *RMSD*=0.3-1m) than for the global (GS512SL4EUK-FCST *RMSD* =0.2-0.8m) model (Fig. 3d). Conversely, AMM15SL2-FCST shows a better performance with a decrease in bias and >20% reduction in *RMSD* compared to the global configuration for T_{02} (Fig. 3g,h). Forecast skill differences are associated with a better

265 representation of bathymetric features, depth related processes and wave-current interaction present in AMM15SL2. The overall contribution of each of these factors is investigated in the next section.

5 Model evaluation

The focus of this paper is to evaluate some of the physical aspects of our operational system in detail. Assessment of the forecast performance showed that the model has a consistent behaviour across lead times, with a degradation in performance

270 that is mostly explained by the wind forcing. We now investigate the performance characteristics of the baseline configurations with a specific focus on the influence of spatial resolution and wave-current interactions using long analysis runs (#AN), herein GS512L4EUK-AN and AMM15SL2-AN (Table 3). Trials covered the period from 1st January 2019 to 31st December 2020 and were based on daily cycles of the models forced by NWP 10km resolution hourly operational winds, between T+0 and T+6 (4 cycles/day), OSTIA sea ice fraction (GS512L4EUK-AN) and AMM15 FOAM 1.5km sea surface currents

275 (AMM15SL2-AN). The trials were initialised from rest with a 10day spin-up period that was discarded. Lateral wave spectral boundary conditions for the AMM15SL2-AN simulation were supplied from the GS512L4EUK-AN simulation. For a detailed evaluation of AMM15 Ocean-Wave Coupled Model and AS512L4EUK wave ensemble refer to Saulter (2020b), Bruciaferri et al. (2021), and Bunney and Saulter (2015), respectively.

Table 3 Experiments specifications for model evaluation.

Experiment	Description
GS512L4EUK-AN	2-year (20190101 to 20201231) analysis run global Forcing: Operational archived hourly NWP 10km resolution updated winds and updated fraction of sea ice. Restart at T+24
AMM15SL2-AN	2-year (20190101 to 20201231) analysis run regional UK waters Forcing: Operational archived hourly NWP 10km updated winds and AMM15 FOAM updated currents. Restart at T+24

280 **5.1 Global spatial and temporal model accuracy**

Global spatial and temporal forcing accuracy is evaluated using altimeter MA_SUP03 (Fig. 4) which provides measurements of wind speed and wave height. The main feature is that there is an underestimation of observed wind speeds by the model (Fig. 4c,d) in those areas that present either small or strong mean wind speeds (Fig. 4a,b), whilst overestimation occurs in mid

latitudes regions with modal observed mean wind conditions (5–10ms^{-1}). Areas which present the lowest mean wind conditions are those across equatorial and close mid latitude regions with very small wind variability (*SD* mean values are of *O*.0.6 ms^{-1}; Fig. 4g,h). Underestimation in these areas seems to be partially linked to sampling bias from the satellite for calm wind conditions. Additionally, very energetic areas such as the Southern part of the Pacific Ocean also present negative bias throughout the year, but these are more exacerbated during JJA months (Fig. 4c; winter in the Southern Hemisphere) during which the largest mean winds are registered. Equally, negative *bias* is present in the northern part of the Atlantic Ocean also corresponding with the strongest winds (average U_{10}>10ms^{-1}) during DJF northern hemisphere winter months (Fig. 4d). As expected, these areas with the strongest winds also present the largest *SDmodel* (>2ms^{-1}) and *RMSD* (1.2ms^{-1}).

Variability for wave metrics match the variability of the wind field, such that larger values of *bias*, *RMSD* and *SDmodel* always correspond with areas with the strongest average wave conditions. A *bias* seasonality is observed with waves underestimated across areas affected by tropical and intra-tropical storms; i.e., tropical, mid and high latitudes in the northern hemisphere during DJF (Fig. 5b,d,f,h) and Indian Ocean during JJA (Fig. 5a,c,e,g). This negative *bias* during stormy seasons turns into a positive one of the same order during periods with calmer average conditions (Fig. 5c,d). Conversely, the southern part of the South Pacific Ocean shows a large variability in the *bias* with no clear seasonality, possibly due to compensating errors. H_s values of *RMSD* oscillate between 0.1–0.3m in most parts of the globe, with a substantial increase to 0.5–0.6m in those areas with the largest mean wave conditions and variability about the mean values (i.e., Southern Ocean during JJA and North Atlantic and North Pacific during DJF). Additional large positive biases around island chains and ice edges are also present, which we attribute to a combination of misrepresentation errors from observation and model. On the one hand, it is acknowledged that satellite measurement errors are larger in complex coastlines and, on the other hand, model resolution and misplacements in the extension of ice sheets will yield in position errors in the wave field. Adopting the GS512L4EUK SMC configuration helped reduce such biases compared to previous configurations (Saulter et al., 2016); however, biases in these areas are still likely due to issues with land/ice masking and the representation of fetch in the model grid.
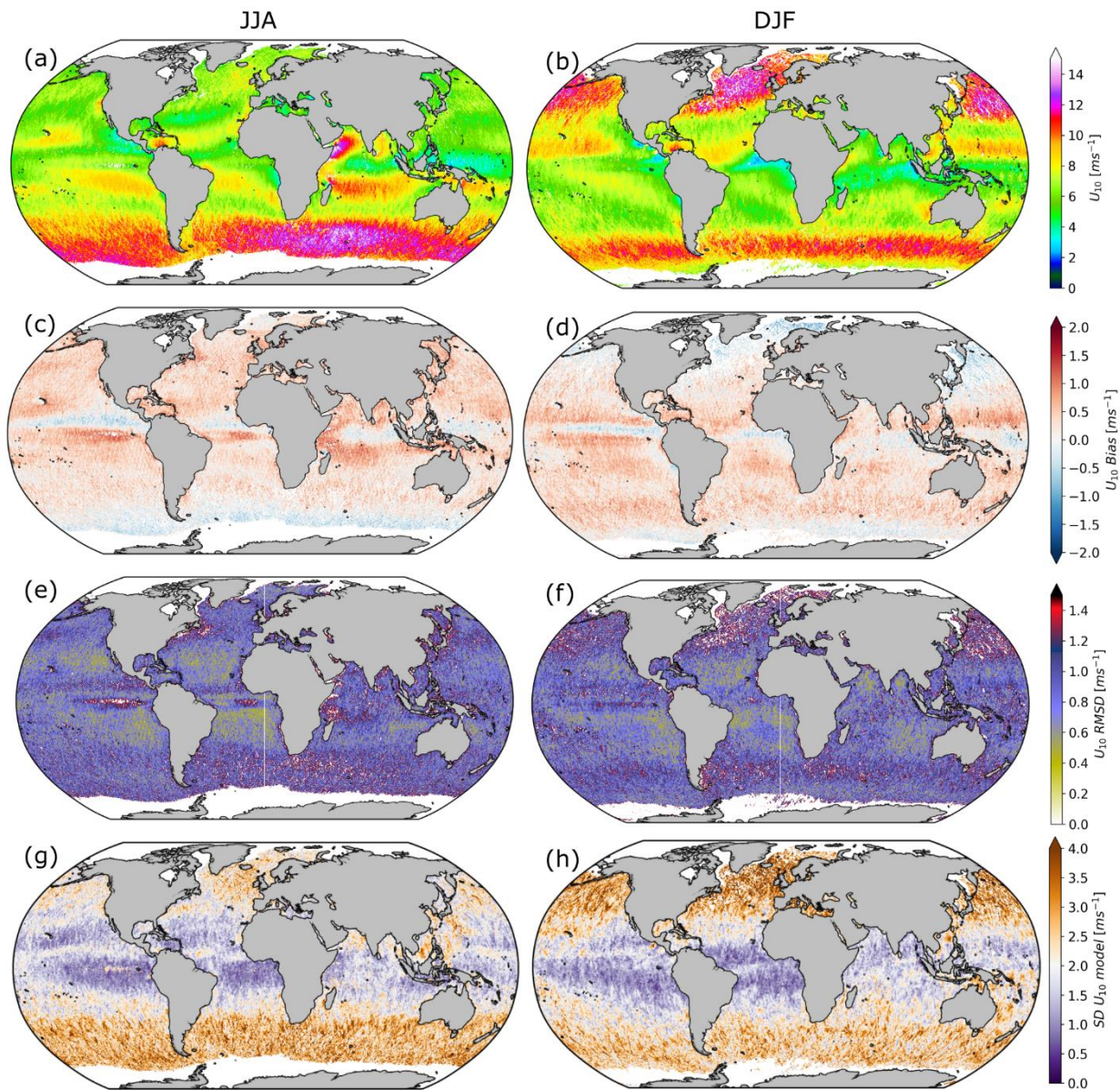
Figure 4. (a,b) Mean, (c,d) *bias* and (e,f) root mean square deviation (*RMSD*) between wind (U₁₀) forcing conditions and merged altimeter observations (MA_SUP03), and (g,h) model standard deviation (*SDmodel*) across the global domain for GS512L4EUK-AN. Stats are aggregated every 15-days and averaged for the months June-July-August (JJA; left column) and December-January-February (DJF; right column).
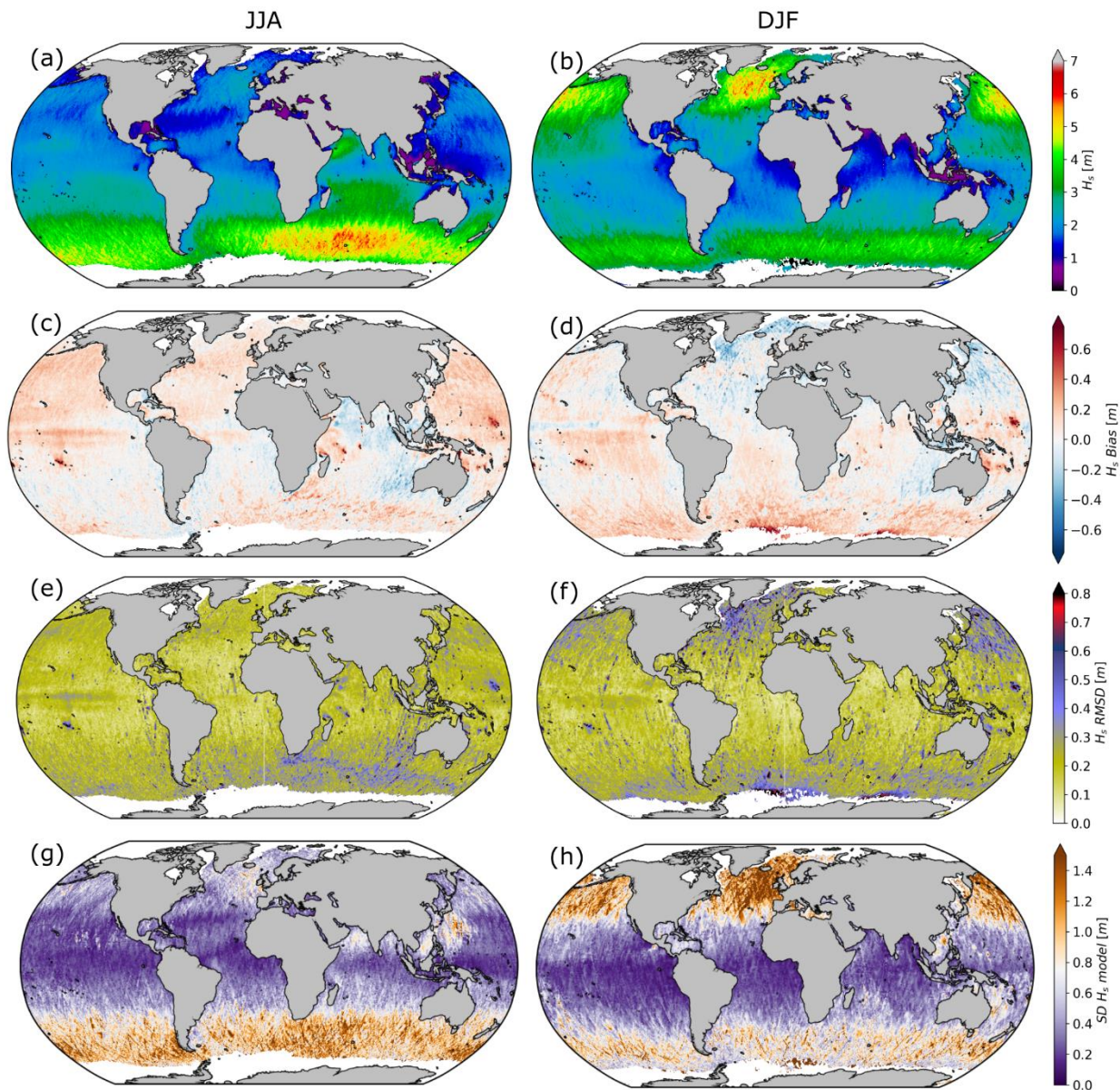
Figure 5. (a,b) Mean, (c,d) *bias* **and (e,f) root mean square deviation (***RMSD***) between modelled significant wave height (H$_s$) and merged altimeter observations (MA_SUP03), and (g,h) model standard deviation (***SDmodel***) across the global domain for GS512L4EUK-AN. Stats are aggregated every 15-days and averaged for the months June-July-August (JJA; left column) and December-January-February (DJF; right column) over 2019-2020.**

Model calibration is based on the best overall performance skill. Figs. 4 and 5 suggest some imbalance during swell dominated conditions in areas such as the Southern Pacific Ocean and the Indian Ocean where winds over this period appear overpredicted whereas significant wave height is consistently underestimated (e.g., waters approaching Western Australia; Fig. 5c,d).

Something similar, albeit to a lesser extent, occurs in tropical and mid latitudes in the western part of the North Atlantic where, despite a slight overestimation of the forcing conditions, the model shows a negative *bias* with respect to altimeter observations.

5.2 Regional spatial and temporal model accuracy

Assessment of AMM15SL2-AN modelled H_s and T_{02} against in-situ observations across the UK waters is presented in Fig. 6. Analysing in-situ observations individually allows us to get a more detailed understanding of caveats on the model performance in the different areas of analysis. Although some metrics vary between summer and winter months, overall, T_{02} seems to be consistently underestimated in most locations (*bias*=-0.5s; Fig. 6g,h) whereas H_s is slightly overestimated (*bias*=0.1–0.2m, Fig. 6e,f). Following the seasonal pattern observed in the global domain, AMM15SL2 model performance is slightly weaker (i.e., larger values of *bias* and *RMSD*) when waves are larger (i.e., DJF). However, conversely to the other metrics, the correlation between model and observations (*r*) is improved during the winter months (average *r* >0.92 versus 0.88 during JJA) suggesting that AMM15SL2 struggles more to replicate the wave energy in the frequency domain during lower energy conditions (H_s=1–2m, T_{02}=5–6s; Fig. 6a–d). Spatially, there are some specific locations where mean *bias*, *RMSD* and *StdE* statistics are consistently large throughout the year (e.g., buoys in the Bristol and English Channels and coastal buoys in very sheltered areas). Whilst the model shows some skill in these regions, the high variability characterised by strong currents due to the tidal range (hypertidal in the case of the Bristol Channel), linked to the fact that those locations are very close to the coast and some local features (e.g., headlands, highly spatially variable bathymetry with features of <3–1.5km spatial scale) are not fully represented by the model, which make these regions very dynamic and difficult to resolve more accurately with the current model configuration.
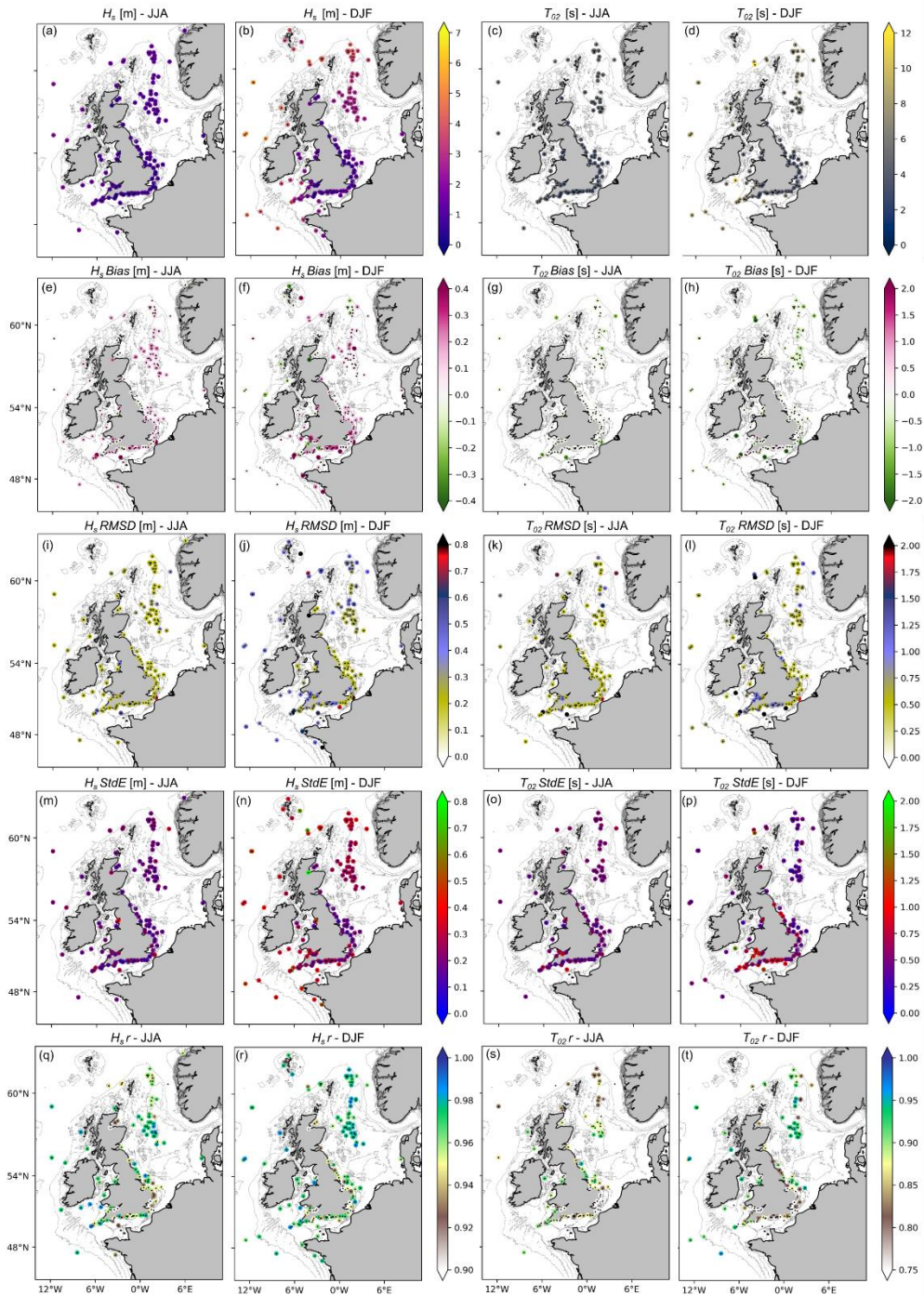
Figure 6. (a–d) Mean, (e–h) *bias*, (i–l) root mean square deviation (*RMSD*), (m–p) standard deviation of error (*StdE*) and (q–t) Pearson correlation coefficient (*r*) between modelled significant wave height (H_s) and mean zero up-crossing period (T_{02}) and in-situ observations across the UK waters domain for AMM15SL2-AN. Stats are computed for the months June-July-August (JJA; left column) and December-January-February (DJF; right column) over 2019–2020. Observations included are JCOMM-WFVS, SHPSYN and WAVENET.

5.3 Comparison of configuration performance

The relative importance of wind and current inputs is presented through evaluations comparing GS512L4EUK-AN and AMM15SL2-AN trials against all observations (i.e., WAVENET, JCOMM-WFVS, SHPSYN and MA_SUP03; Table 3). Overall metrics are computed for the individual domains, i.e. the entire globe and the NW shelf – UK waters area respectively. Note that evaluation of wave direction (Dir) only corresponds to the coastal waters of the UK.

Table 3. Summary statistics for wind speed (U_{10}), wind direction (U_{10} dir), significant wave height (H_s), mean zero up-crossing period (T_{02}) and wave direction (Dir): GS512L4EUK-AN and AMM15SL2-AN versus observations of WFVS, SHPSYN, WAVENET and merged altimeter (MA_SUP03) over 20190101 to 20201231.

| | | GS512L4EUK-AN | | | | | | AMM15SL2-AN | | | | | |
Variables	Observations	Mean	Bias	RMSD	StdE	SS	r	Mean	Bias	RMSD	StdE	SS	r
U_{10}	WFVS	7.19	0.26	2.00	1.98	1.13	0.86	8.27	0.20	2.20	2.19	1.06	0.84
	SHPSYN	8.19	0.34	1.63	1.59	0.97	0.92	8.19	0.34	1.62	1.58	0.97	0.92
	WAVENET	-	-	-	-	-	-	-	-	-	-	-	-
	MA_SUP03	7.87	0.26	1.49	1.46	1.05	0.92	8.47	0.36	1.36	1.31	1.09	0.95
U_{10} dir	WFVS	-	0.83	23.05	23.04	0.99	-	-	0.49	14.36	14.36	1.01	-
	SHPSYN	-	-1.32	19.92	19.88	0.99	-	-	-1.27	19.65	19.61	0.99	-
	WAVENET	-	-	-	-	-	-	-	-	-	-	-	-
	MA_SUP03	-	-	-	-	-	-	-	-	-	-	-	-
H_s	WFVS	1.88	0.05	0.29	0.29	0.95	0.97	2.08	0.09	0.28	0.26	0.95	0.98
	SHPSYN	2.09	0.12	0.33	0.31	0.93	0.97	2.09	0.12	0.32	0.30	0.91	0.97
	WAVENET	1.25	0.02	0.32	0.32	1.02	0.94	1.25	0.06	0.26	0.25	0.99	0.96
	MA_SUP03	2.74	0.05	0.35	0.35	0.95	0.97	2.71	0.02	0.32	0.32	0.93	0.98
T_{02}	WFVS	6.31	-0.80	1.41	1.16	0.60	0.79	6.15	-0.56	0.99	0.82	0.62	0.88
	SHPSYN	5.98	-0.58	0.99	0.80	0.71	0.86	5.98	-0.56	0.98	0.80	0.69	0.87
	WAVENET	4.52	-0.24	0.78	0.74	1.19	0.86	4.52	-0.12	0.67	0.66	1.15	0.89
	MA_SUP03	-	-	-	-	-	-	-	-	-	-	-	-
Dir	WFVS	-	-	-	-	-	-	-	-	-	-	-	-
	SHPSYN	-	-	-	-	-	-	-	-	-	-	-	-
	WAVENET	-	-0.01	32.79	32.79	0.97	-	-	-1.55	27.58	27.54	0.97	-
	MA_SUP03	-	-	-	-	-	-	-	-	-	-	-	-

One of the main factors that influence the reliability of a wave spectral model is the accuracy of the forcing conditions. Modelled wind forcing is compared against observations in order to assess their consistency for the baseline configurations (Table 4). Interestingly, differences in U_{10} metrics are not significant, indicating that wind forcing conditions are steady and suggesting that the wind interpolation to the underlying regular grid with the coarsest SMC resolution (25km for GS512L4EUK and 3km for AMM15SL2) does not degrade the overall wind speed performance. However, U_{10} dir compares closer to observations for the AMM15SL2 domain (*RMSD*=21.49º and 17.00º, *StdE*=21.46º and 16.98º for GS512L4EUK and

AMM15SL2 respectively) demonstrating that errors between modelled U_{10} dir and observations are both smaller and more representative of the wind conditions across the NW shelf. (i.e., when the original spatial variability of the 10km winds is retained and not upscaled).

360 The incorporation of ocean surface currents in the wave model aims to improve modelled sea states (e.g., Hersbach and Bidlot, 2008; Palmer and Saulter, 2016; Ardhuin et al., 2017; Alday et al., 2022). Analysing the observations as a whole (average values), statistics show excellent model accuracy predicting H_s even when currents are not included (i.e., GS512L4EUK). Both baseline configurations present very good correlation coefficients (H_s r=0.94–0.97 and T_{02} r=0.84–0.88 for GS512L4EUK-AN and AMM15SL2-AN, respectively; Table 3), mean SS (0.95–0.96; i.e., $SDobs$ is larger than $Sdmodel$) and small positive

365 *biases* for H_s (0.06m and 0.07m) and negative for T_{02} (*bias* = -0.54--0.41s). When comparing differences in performance only for the NW shelf – UK waters (Fig. 7), results show that although there is a positive impact of the surface currents and increased resolution, with 5% MSE decrease in coastal locations (i.e., WAVENET, Fig. 7), this is not always present in the overall statistics of H_s, and neutral changes and even some degradation exists in specific locations (overall 1 and 5% increase in *MSE* and *bias*).

370 The increased resolution in AMM15SL2, together with the refraction produced by tidal currents, help to better capture mean period and wave direction near the coast where bathymetric changes and coastal obstructions are better resolved (Fig. 7). AMM15SL2-AN shows an acceptable performance in all the coastal areas of analysis with Dir *RMSD* values oscillating from 17º–32º which corresponds to 25% of the observation standard deviation. This percentage in the *RMSD* increases to 36% for the case of GS512L4EUK-AN. A further contribution to the improved wave direction fields in AMM15SL2 is also expected

375 from the wind interpolation. Model accuracy improvement for T_{02} is more than 2–9% on average *MSE* and *bias* (Table 3) with >20% reduction in *RMSD*. This overall improvement in the mean period for AMM15SL2-AN is even more significant in most coastal locations despite some exceptions such as the Scarweather directional wave buoy (Bristol Channel) where, although the tidal modulation of the wave field is only captured by AMM15SL2-AN, it leads to a larger spread in the observation-model differences.

AMM15SL2-AN vs GS512L4EUK-AN
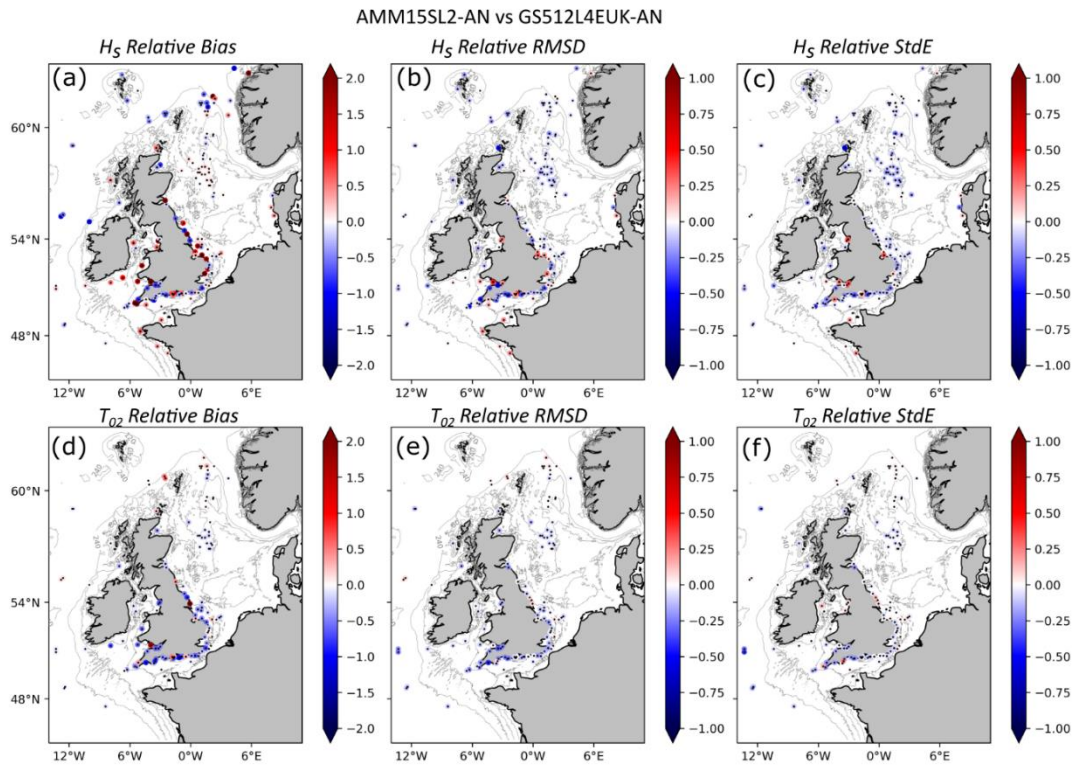
Figure 7. Relative change in absolute *bias* (a,d), *RMSD* (b,e) and *StdE* (c,f) between observations-model comparison for AMM15SL2-AN and GS512L4EUK-AN for significant wave height (H_s) and mean period (T_{02}) across UK waters. Stats are computed over 2019–2020 and observations included are JCOMM-WFVS, SHPSYN and WAVENET. Negative (positive) values indicate a reduction (increase) of the metric by AMM15SL2-AN. To facilitate visualisation when no relative change is observed, all in-situ locations are indicated with a black dot.

5.4 Wave-current interaction

The addition of surface currents has effects on wave generation, advection and refraction, with the latter being one of the main wave-current processes affecting the wave field in areas with large tidal currents such as those on the shelf. We focus now on areas where the tide has a dominant effect on the wave field using WAVENET in-situ directional wave buoys.

When comparing GS512L4EUK and AMM15SL2, we show that wave-current interaction in areas where tidal currents are important produces larger wave heights and positive changes in the wave period and direction. An example of these fluctuations is presented at Start Bay wave buoy (Fig. 8) which is a tide modulated coastal in-situ location in the English Channel. Adding the wave-current interactions leads to a reduction of the small negative H_s *bias* at this site from -0.11 to -0.02 m with a reduction of the *RMSD* from 0.2m to 0.14m. The quantile-quantile relationship (QQ) for H_s at this location shows that both configurations are in very good agreement with observations (r=0.95 and 0.97 for GS512L4EUK-AN and AMM15SL2-AN, respectively) and both tend to underestimate the tail of the distribution; however, this is much closer to observations in AMM15SL2-AN. T_{02} QQ shows an underprediction of the lower periods (T_{02}=2–6s with *bias*=0.5–1s; Fig. 8c,d) and a significant overestimation

of larger periods (T_{02}>8s) that is accentuated in the regional configuration. Despite this, overall T_{02} metrics are improved when currents are accounted for. In line with the improvement of Dir by AMM15SL2-AN present in most coastal locations, Dir
400   *RMSD* at Start Bay is significantly reduced from 44º to 32.25º and this is reflected in a significant reduction of the model biases.
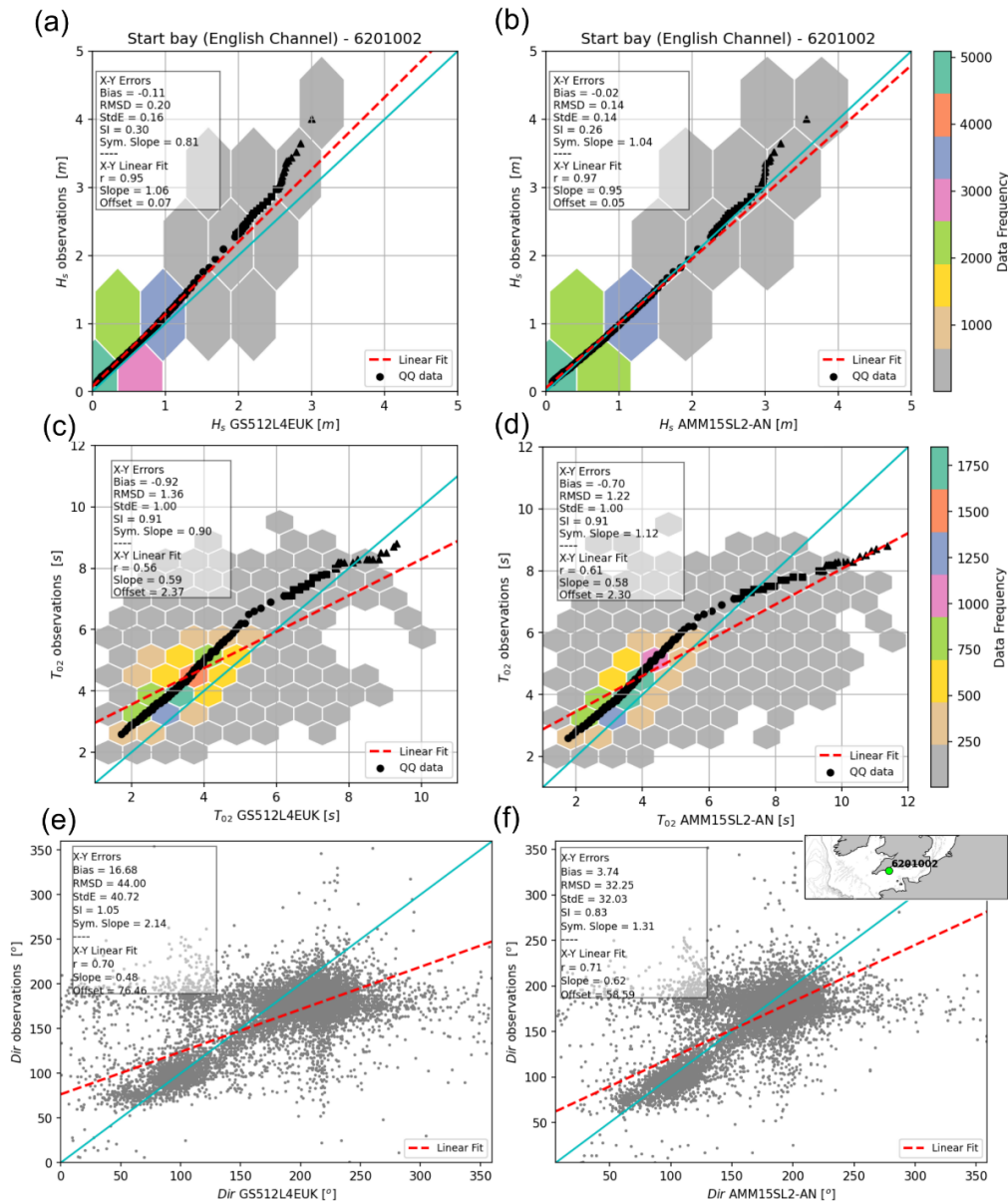
Figure 8. (a,b) Significant wave heigh (H_s) and (c,d) mean period (T_{02}) quantile-quantile relationship and scatter data for GS512L4EUK-AN (left column) and AMM15SL2-AN (right column) at Start Bay in-situ wave buoy. (e,f) Scatter plots for wave
405   **direction (Dir) at Start Bay in-situ wave buoy. Inset with wave buoy location is presented in panel (f). Wave bulk stats are included in each individual panel and correspond to the comparison between model and observations over 20190101 to 20201231.**

Tidal modulation of the wave field is observed in several locations. As an example that is representative of most coastal areas, Fig. 9 shows the timeseries of H_s, T_{02} and Dir for both configurations at the Scarweather wave buoy, located in the Bristol Channel, where an increase in the observed T_{02} and H_s can be seen during each tidal cycle (Fig. 9a,b). This modulation is only present in the AMM15SL2 configuration; however, sometimes a lag in the tidal fluctuation (3h for Scarweather; up to 6h in other locations) occurs between model and observations that may lead to poorer metrics than when no currents are used (i.e. the run without currents provides a smoother signal). In line with some additional forcing evaluation of the current field (refer to *Supplementary material*), this lag is linked to the negative veering (tidal phase) that is present in the modelled currents where observations tidal velocities lead the model velocities. Equally, it is also noted the importance of the tidal modulation on the wave direction present in AMM15SL2-AN timeseries captured on the observations within a range of +/-30 degrees (Fig. 9c) in these coastal wave buoys.
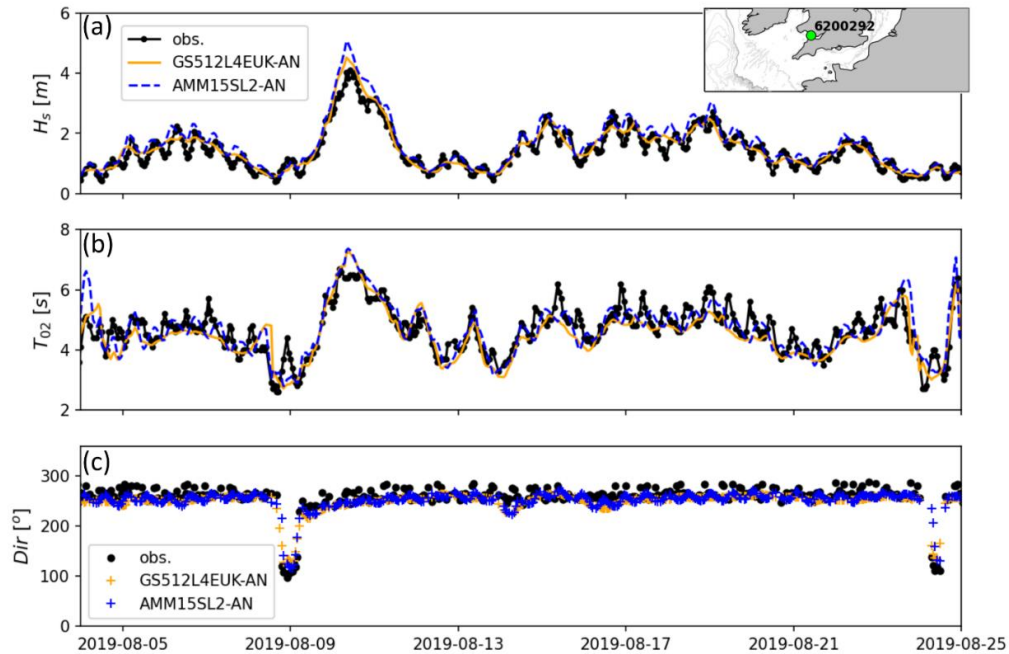
Figure 9. Timeseries of (a) significant wave heigh (H_s), (b) mean period (T_{02}) and direction (Dir) for GS512L4EUK-AN and AMM15SL2-AN (right column) at Scarweather in-situ wave buoy. Inset with wave buoy location is presented in panel (a).

Differences in the accuracy of both configurations suggests that wave refraction and shifts in the relative frequency are better captured with the addition of the sea surface currents in most of the domain. However, overall metrics for H_s are slightly weaker in certain areas of analysis such as the Irish and Celtic Seas, English and Bristol Channel and E coast of England. To isolate the effect of currents and not account for any differences in resolution, we run the AMM15SL2 configuration without currents during August 2019 and compare model differences in H_s over two tidal cycles during spring tides (Fig. 10a). Positive residual differences in H_s correspond to those locations where AMM15SL2 presents some degradation respect GS512L4EUK. Model evaluation showed that both configurations tend to slightly overestimate H_s, therefore, the overall positive bias is

exacerbated by the contribution of the residual currents in AMM15SL2. Additionally, the evaluation of the currents effects on the wave energy distribution in two different shallow coastal locations demonstrate that including tidal currents produces a consistent shift towards longer periods (Fig. 10e,g) reducing the energy bias between model and observations at low

430   frequencies (not shown), hence the better agreement for the period in AMM15SL2. In terms of Dir, model differences during ebb (Fig. 10b) and flood (Fig. 10c) tide conditions show wave refraction angles of $\pm10^{\circ}$ when currents are included, helping to better capture the distribution of the wave energy in the directional space (e.g., Fig. 8f). This suggests that AMM15SL2 captures the distribution of the energy in terms of frequency and direction better whereas the total energy might be sometimes too large in this configuration. In other words, the bulk energy imparted to the ocean surface waves might be excessive during

435   low-moderate conditions.
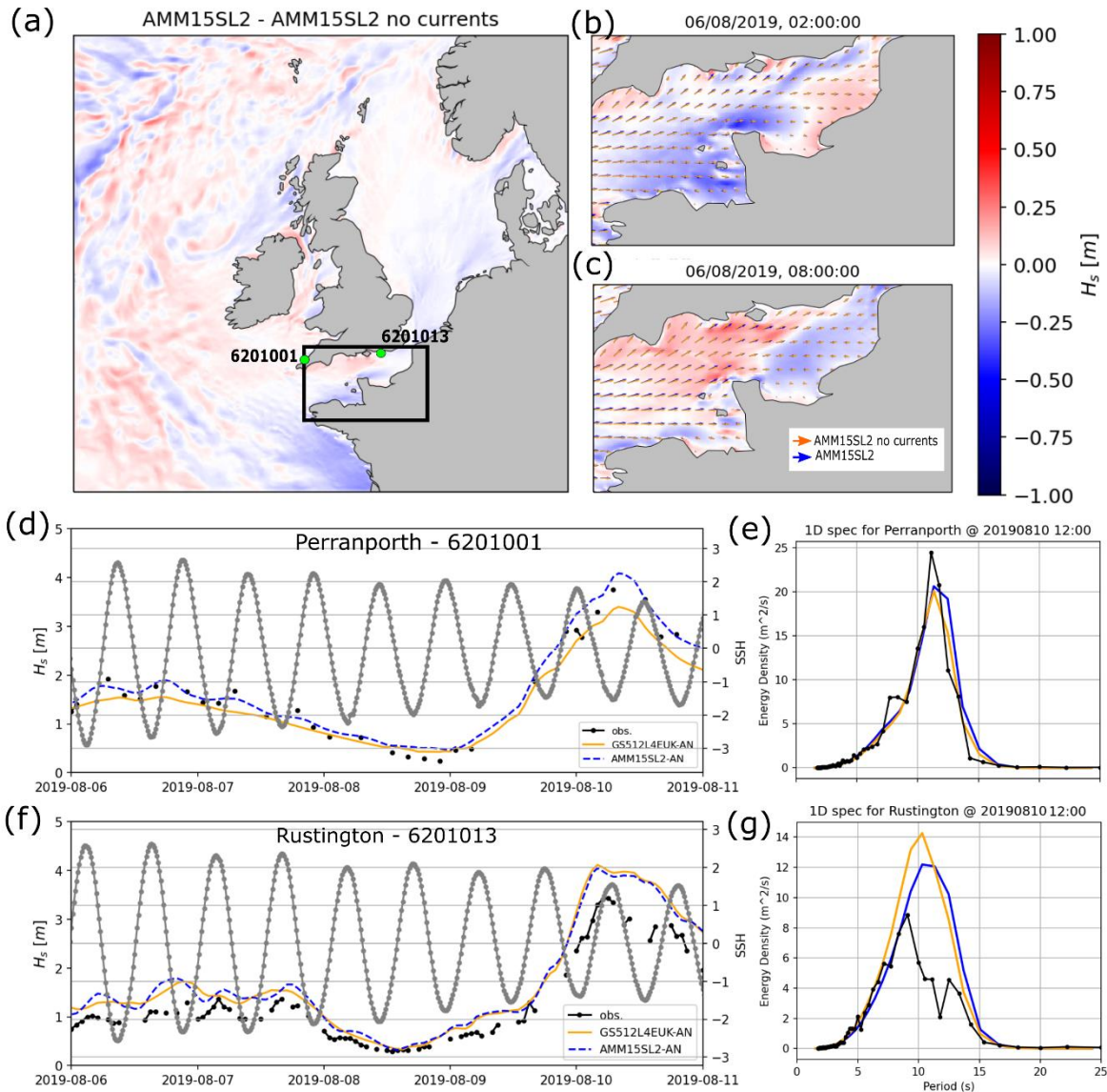
Figure 10. Effects of currents in significant wave height (H$_s$). (a) Mean difference over two tidal cycles (25h) between AMM15SL2 and GS512L4EUK for H$_s$ (a) across UK waters. (b,c) Snapshots of H$_s$ difference over the English Channel (see panel (a) for zoom reference) during ebb (b) and flood tide (c) conditions with vectors for wave direction. (d,f) Timeseries of sea surface height (SSH) and Hs and (e,g) 1D spectra in Perranporth (6201001) and Rustington (6201013) directional waveriders during a storm event in August 2019. Wave buoy locations are presented in panel (a).

5.5 Impact of resolution on wave growth

Increased resolution has been demonstrated to play an important role in model skill score. However, the advantages of using higher spatial resolution in AMM15SL2 do not always show in the overall skill of H$_s$. It is known that model simulations can show significant sensitivity to spatial resolution and source term model set-up. All configurations in the Met Office wave

forecast system include the same source term tuning parameters (refer to *Supplementary material*) as this has been found to be suitable in previous system versions. To test the sensitivity of spatial resolution, we run a number of WW3 idealised numerical experiments with variable resolution. The domain has an extent of 1000km x 500km that is discretised with regular grids of 10km, 5km and 2.5km resolution; experiments 10kmRes, 5kmRes and 2.5kmRes, respectively. All resolutions are then

450   explored for deep water (flat bathymetry of 1000m depth) and shallow water (flat bathymetry of 40m deep) conditions. The model is forced for 48h by a constant wind speed ranging from 10 to 30ms^{-1}. All simulations include the same source term configuration and tuning terms.

Dimensionless fetch limited growth (gH_s/U_{10}^2) curves as a function of dimensionless fetch ($gfetch/U_{10}^2$) for the different idealised experiments are presented in Fig. 11. For reference, the theoretical wave growth relationships derived from

455   observations by Young and Verhagen (YV96; Young and Verhagen, 1996) are also included. The difference in wave growth between resolutions is greater for shorter fetches and lower winds. High resolution grids (i.e., 2.5kmRes) generate higher waves compared to YV96 relationship for both deep (Fig. 11a,c,e) and shallow (Fig. 11b,d,f) water. This behaviour for short fetches is consistent for all wind speeds with higher resolution resulting in larger growth rates. In all cases differences between resolutions become smaller as wind speed increases. Idealised experiments suggest that the increased resolution in

460   AMM15SL2-AN might lead to faster wave growth and subsequently larger H$_s$ for mid to high-energy wind conditions in fetch-limited areas. Accordingly, model-observation results show that for modal conditions, although both models tend to slightly overestimate H$_s$, neutral or some skill weakening reproducing H$_s$ is observed in AMM15SL2-AN. Conversely, extremes, although generally underestimated (not shown), tend to be better replicated by AMM15SL2-AN mainly in fetch limited locations (e.g. at Start Bay; Fig. 8a,b). The implication is that to obtain a similar behaviour in all model configurations, the

465   next generation of Met Office modelling systems should include a modified parameterization that is domain dependent as the current source term set-up is more optimised for GS512L4EUK configuration and modal conditions.
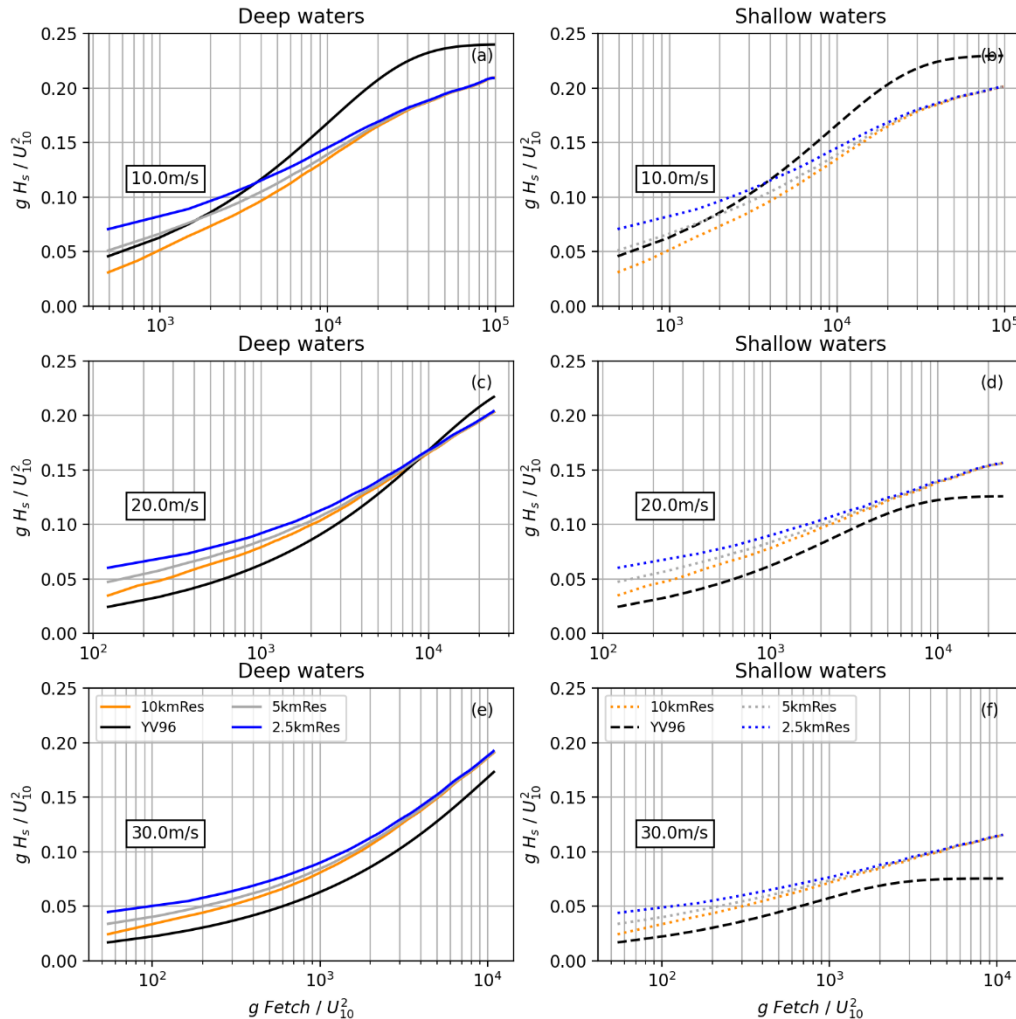
Figure 11. Dimensionless wave growth curves for different model grid resolutions (10km, 5km and 2.5km) as a function of dimensionless fetch. Fetch limited growth curves are computed for (a,c,e) deep water and (b,d,f) shallow water (40m depth) for constant winds of 10, 20 and 30ms⁻¹. The theoretical curve of Young and Verhagen (1996) is presented (YV96). Results for the different configurations correspond to 48h model runs.

6 Discussion and ongoing development

We have presented a comprehensive evaluation of two of the Met Office operational wave configurations: the global GS512L4EUK and the regional AMM15SL2. Both models show good performance when compared to different observation datasets and this skill is retained for all lead times in the forecast. We have illustrated the benefits of the SMC grid, that allows to resolve the propagation in open waters at lower resolution and to incorporate the effect of complex bathymetry and coastline as waves approach to shore. We put particular attention in studying two relevant aspects that describe the benefits provided by AMM15SL2: the impact of incorporating currents and the implications of higher resolutions in wave growth.

Recent studies have demonstrated positive impacts on significant wave height prediction when surface ocean currents are
480   accounted for (e.g., Palmer and Saulter, 2016; Ardhuin et al., 2017; Echevarria et al., 2021; Valiente et al., 2021b). AMM15SL2
based configuration includes wind and sea surface currents as forcing conditions. Accurate representation of the wave-current
interactions across the NW shelf - UK waters domain is essential as ocean-wave coupling improves accuracy of the ocean
surface dynamics by 4% (Bruciaferri et al., 2021). Additionally, it is clear that the presence of currents can modify the
distribution of the wind waves on the shelf with >15% impact during modal conditions (e.g., Ardhuin et al., 2017; Valiente et
485   al. , 2021b; Alday et al., 2022). Although relative changes in T_{02} metrics and wave Dir show an overall significant improvement
(>25% in *RMSD* and 10% in *bias*), the quantitative assessment to demonstrate the improvement of the forecast skill in the
significant wave height diagnostic by AMM15SL2 with respect to GS512L4EUK proves difficult in some instances. The lag
between model and observations present in some in-situ locations due to the tidal modulation (i.e., larger spread on the
observation-model differences and possible double penalty effect; Crocker et al., 2020), together with an excessive bulk energy
490   imparted to the ocean surface waves in AMM15SL2 configuration (consequence of the numerical choice), led sometimes to
poorer metrics than when no currents and higher resolution are used (i.e., GS512L4EUK).

Discretization and numerical schemes (e.g., Roland and Ardhuin, 2014), together with forcing accuracy and the choice of the
parameterisation for wave growth and dissipation (e.g., Ardhuin et al., 2010; Zieger et al., 2015) are among the main factors
affecting the accuracy of a spectral model (e.g., Alday et al., 2022). In our evaluation, we show that resolution and the choice
495   of the numerical tuning significantly influences the model accuracy. Furthermore, model skill improvement representing
modal/ extreme conditions can be optimised but often leads to degradation of part of the distribution of the wave field. Met
Office configuration changes from ST4 source term defaults included a combination of a reduction of the sheltering for short
waves (TAUWSHELTER term) and a bulk adjustment to the wind field through a decrease of the maximum value allowed for
wind-wave coupling (BETAMAX term), leading to an increase in model accuracy reproducing the tail of the distribution that
500   subsequently led to some degradation in those sectors where the model was already overestimating.

The latest developments and performance of the current Met Office operational wave system has been presented. Imminent
system developments will incorporate:

- Use of sea point wind forcing in the SMC grid, improving the wind transfer between atmosphere and ocean. The
change in the pre-processing of the wind forcing conditions task will include sea point winds (i.e., SMC grids cells)
505   instead of the current pre-processing step where winds are interpolated to the underlaying grid resolution (25km for
GS512L4EUK and 3km for AMM15SL2) in which 10km NWP Met Office wind resolution for the global domain is
up-scaled. This development will help correcting some of the wave model behaviour in areas of the globe where an
improvement in wind speed and direction due to the higher resolution interpolation is likely to be an important factor.

- Optimisation of the models in line with model resolution. Idealised scenarios showed resolution dependent wave
510   growth indicating that it is important to optimise the source term parameterisation for the different spatial resolutions.
Model-observation errors observed in AMM15SL2 for modal conditions are expected to be reduced after the retuning

of the regional model to better match observations across the coastal UK waters as currently this is more optimised to better capture extremes and for the global model.

- SMC multigrid. Implementation of a multigrid approach for the global domain that will allow for improved scaling and hybrid parallelisation (component and domain decomposition) in hybrid MPI-OpenMP mode.

Future systems will include the waves as a system component of a more comprehensive atmosphere-wave-ocean-land-ice system. This implies, in most cases, a need to develop more integrated systems where the different physical components (i.e., atmosphere, ocean, ice and waves) are coupled (e.g., Lewis et al., 2019; Bruciaferri et al., 2021; Valiente et al., 2021a; Castillo et al., 2022). In recent years, the Met Office has put significant effort into the development of fully coupled models and although an operational AMM15 ocean-wave coupled system has been deployed, more complex atmosphere-wave-ocean coupled models are currently in a pre-operational research phase. The GS512L4EUK wave model described in this paper is in the process of being implemented in a global research atmosphere-ocean-ice-wave coupled configuration; however, it will need time before it becomes operational. For the case of the operational AMM15 ocean-wave coupled with data assimilation, this is currently run once a day providing 5 days forecast. This is still computationally expensive with increased resource demands over the wave-only operational model with currents as forcing that delivers data four times a day. Met Office internal testing demonstrates that a coupled simulation increases 10% the running time per model respect their standalone version; i.e., if an ocean model needs n nodes to run and a wave model needs m nodes, the ocean-wave coupled simulation of the two will need $n+m$ nodes with an increase of 20% in the running time. While studies continue toward a fully coupled prediction system with atmosphere, ocean, land, ice and wave components, the maintenance and development of each of the model components is crucial in NWP.

7 Conclusions

The latest developments and performance of the current Met Office operational wave model forecasting system, focused on the global (GS512L4EUK) and the NW shelf - UK waters (AMM15SL2) baseline configurations have been presented. Model-observations correlation is beyond 0.94–0.96 in all areas of analysis with standard deviations of differences that correspond to maximum 13–25% of the observed mean bulk wave diagnostics, demonstrating the quality and accuracy of the Met Office wave forecast capability. This showcases the benefits of the SMC grid, a Met Office development, which provides computational efficiency while retaining good performance when compared to observations at both global scale and near shore. Met Office configurations are optimised to accurately predict modal conditions with a tendency to slightly overestimate. We show that tidal currents produce a residual signal that presents a more realistic looking wave time-series but can affect the final accuracy of the model. That is, areas where the tidal currents increase (decrease) the significant wave height led to some degradation (improvement) of this parameter by AMM15SL2.

The inclusion of wave-current effects and the higher resolution for depths <40m in AMM15SL2 together with a better representation of the local features (e.g., headlands, highly spatially variable bathymetry) result in an incremental improvement in the representation of the wave field mainly in the frequency and directional domain. The prediction of the wave direction near the coast is improved within a range of +/-30 degrees and the mean period shows >20% reduction in the RMSD with respect to GS512L4EUK. This is also a consequence of the increase in wind forcing resolution (10km), as winds in AMM15SL2 are not presently up-scaled in the pre-processing routine performed for GS512L4EUK (i.e., 10km resolution winds are interpolated to a 25km regular grid).

We demonstrate that resolution and the choice of the numerical tuning significantly influences the model accuracy. Evidence of resolution dependent differences in wave growth was observed, leading to slightly overestimated significant wave heights when replicating coastal mid-range conditions by AMM15SL2. This is better suited to replicate the extremes, particularly on regions with short and mid fetches such as the North Sea.

The improved skill of AMM15SL2, together with a better prediction of mean upcrossing period and wave direction, has large implications for the prediction of waves in shot fetched areas and coastal locations. This provides benefits for both off-shore infrastructures, such as wind power or oil platforms, as well as in coastal applications like beach safety, risk to flooding and overtopping and shoreline evolution in general. It is also recognised that, despite a good skill of AMM15SL2 in replicating inshore waves, the model utility in coastal zones largely sheltered and/or with strong shallower water bathymetric variability should be treated with caution as there are important non-linear effects that are not included in any of the baseline configurations.

Data availability. The length, resolution and spatial coverage of the data generated in running the trials described in this paper requires a large storage facility. The complete or partial data will be available via request to the corresponding author. Data used for the model evaluation and analysis in this paper in the form of model-observations match-up netCDF files are available via https://doi.org/10.5281/zenodo.7019826.

Datasets for model evaluation include different sources. SHPSYN in-situ observations is accessed via the Global Telecommunication System but it is also publicly available via http://www.marineinsitu.eu/dashboard/. WAVENET in-situ data is obtained from the National Network of Regional Coastal Monitoring Programmes and CEFAS Wavenet, and should be available prior registration at http://www.channelcoast.org/ and https://www.cefas.co.uk/cefas-data-hub/wavenet/. JCOMM-WFVS observations are obtained as Met Office is part of the World Meteorological Organisation - International Oceanographic Commission (WMO-IOC) Joint Commission On Marine Meteorology's operational Wave Forecast Verification Scheme. MA_SUP03 satellite altimeter data is available for public download and can be obtained prior registration via FTP in ftp://ftp.ifremer.fr/ifremer/cersat/products/swath/altimeters/waves/data.

Additional information on the data acquisition of the different observational datasets used in this paper is included in the *Supplementary material.*

Code availability - Obtaining WAVEWATCH III®. The version of WAVEWATCH III used operationally at the Met Office is publicly available via the Met Office's "Trusted Institutional Fork" of the NOAA WW3 GitHub repository: https://github.com/ukmo-waves/WW3/tree/ukmo_ps45-1.hotfixes. The WAVEWATCH III code base is distributed by NOAA under an open-source style licence via http://polar.ncep.noaa.gov/waves/wavewatch/wavewatch.shtml (NOAA, 2021a). Interested readers wishing to access the code are requested to register to obtain a license via http://polar.ncep.noaa.gov/waves/wavewatch/license.shtml (NOAA, 2021b). Refer to Supplementary material for more details.

Code availability - Obtaining configuration files. Basics of the system configuration including grid, modules and tuning parameters files are publicly available via https://doi.org/10.5281/zenodo.7148687.

Author contributions. N. G. V. conceptualised the experiments, set-up and run baseline trials, conducted the formal analysis and wind and wave verification as well as data curation, wrote the original draft and prepared figures/visualization; A. S. and B. G. helped with conceptualisation, validation resources and review and editing of draft; C. B. and J. L. contributed to model description and provided a figure for SMC visualisation; C. P. performed AMM15 currents validation; C. B., A. S., J. L., N. G. V. and T. P. contributed to the development of the wave operational system. All the co-authors contributed to the edition of the final version of the manuscript.

Competing interest. The authors declare that they have no conflict of interest.

References

Alday, M., Ardhuin, F., Dodet, G., and Accensi, M.: Accuracy of numerical wave model results : Application to the Atlantic coasts of Europe, Ocean Science, 18(6), 1665-1689, https://doi.org/10.5194/os-18-1665-2022, 2022.

Ardhuin, F., Gille, S. T., Menemenlis, D., Rocha, C. B., Rascle, N., Chapron, B., Gula, J., and Molemaker, J.: Small-scale open ocean currents have large effects on wind wave heights, Journal of Geophysical Research: Oceans, 122(6), 4500–4517, https://doi.org/10.1002/2016JC012413, 2017.

Ardhuin, F., Rogers, E., Babanin, A., Filipot, J.-F., Magne, R., Roland, A., Queffelou, P., Lefevre, J. M., Aouf, L., Babanin, A., and Collard, F.: Semi-empirical dissipation source functions for wind-wave models: part {I}, definition, calibration and validation, J. Phys. Oceanogr., 40(9), 1917–1941, 2010.

Ardhuin, F., Roland, A., Dumas, F., Bennis, A.-C., Sentchev, A., Forget, P., Wolf, J., Girard, F., Osuna, P., and Benoit, M.: Numerical Wave Modeling in Conditions with Strong Currents: Dissipation, Refraction, and Relative Wind, Journal of Physical Oceanography, 42(12), 2101–2120, https://doi.org/10.1175/JPO-D-11-0220.1, 2012.

Battjes, J. A., and Janssen, P.: Energy loss and set-up due to breaking of random waves, Coastal Engineering, 569–587, https://doi.org/10.9753/icce.v16, 1978.

610 Bidlot, J., Wittmann, P., Fauchon, M., Chen, H., Lefèvre, J. M., Bruns, T., Greensdale, T., Ardhuin, F., Kohno, N., and Park, S.: Inter-comparison of operational wave forecasting systems, 10th International Workshop on Wave Hindcasting and Forecasting and Coastal Hazard Symposium, North Shore, Oahu, Hawaii, 1–22, 2007.

Booij, N., and Holthuijsen, L. H.: Propagation of ocean waves in discrete spectral wave models, Journal of Computational Physics, 68(2), 307–326, https://doi.org/10.1016/0021-9991(87)90060-X, 1987.

615 Brown, A., Milton, S., Cullen, M., Golding, B., Mitchell, J., and Shelly, A.: Unified modeling and prediction of weather and climate: A 25-year journey, Bulletin of the American Meteorological Society, 93(12), 1865–1877, https://doi.org/10.1175/BAMS-D-12-00018.1, 2012.

Bruciaferri, D., Tonani, M., Lewis, H. W., Siddorn, J. R., Saulter, A., Castillo Sanchez, J. M., Valiente, N. G., Conley, D., Sykes, P., Ascione, I., and McConnell, N.: The Impact of Ocean-Wave Coupling on the Upper Ocean Circulation During
620 Storm Events, Journal of Geophysical Research: Oceans, 126(6), https://doi.org/10.1029/2021JC017343, 2021.

Bunney, C., and Saulter, A.: An ensemble forecast system for prediction of Atlantic-UK wind waves, Ocean Modelling, 96, 103–116, https://doi.org/10.1016/j.ocemod.2015.07.005, 2015.

Castillo, J. M., Lewis, H. W., Mishra, A., Mitra, A., Polton, J., Brereton, A., Saulter, A., Arnold, A., Berthou, S., Clark, D., Crook, J., Das, A., Edwards, J., Feng, X., Gupta, A., Joseph, S., Klingaman, N., Momin, I., Pequignet, C., Sanchez, C., Saxby,
625 J., and Valdivieso da Costa, M.: The Regional Coupled Suite (RCS-IND1): application of a flexible regional coupled modelling framework to the Indian region at kilometre scale, Geosci. Model Dev., 15, 4193–4223, https://doi.org/10.5194/gmd-15-4193-2022, 2022.

Cavaleri, L., and Rizzoli, P. M.: Wind Wave Prediction in Shallow Water: Theory and Applications, Journal of Geophysical Research, 86(C11), 10,961-10,973, https://doi.org/10.1029/JC086iC11p10961, 1981.

630 Crocker, R., Maksymczuk, J., Mittermaier, M., Tonani, M., and Pequignet, C.: An approach to the verification of high-resolution ocean models using spatial methods, Ocean Science, 16(4), 831–845, https://doi.org/10.5194/os-16-831-2020, 2020.

Echevarria, E. R., Hemer, M. A., and Holbrook, N. J.: Global implications of surface current modulation of the wind-wave field, Ocean Modelling, 161(March 2020), 101792, https://doi.org/10.1016/j.ocemod.2021.101792, 2021.

Good, S., Fiedler, E., Mao, C., Martin, M. J., Maycock, A., Reid, R., … Worsfold, M.: The current configuration of the OSTIA
635 system for operational production of foundation sea surface temperature and ice concentration analyses, Remote Sensing, 12(4), 1–20, https://doi.org/10.3390/rs12040720, 2020.

Graham, J. A., O'Dea, E., Holt, J., Polton, J., Hewitt, H. T., Furner, R., Guihou, K., Brereton, A., Arnold, A., Wakelin, S., Castillo Sanchez, J. M., and Mayorga Adame, C. G.: AMM15: a new high-resolution NEMO configuration for operational simulation of the European north-west shelf, Geosci. Model Dev., 11, 681–696, https://doi.org/10.5194/gmd-11-681-2018,
640 2018.

Gurgel, K.-W., Schlick, T., Voulgaris, G., Seemann, J., and Ziemer, F.: HF radar observations in the German Bight:

Measurements and quality control, IEEE/OES 10th Current, Waves and Turbulence Measurements (CWTM), 51–56. https://doi.org/10.1109/CWTM.2011.5759524, 2011.

645 Hasselmann, K., Barnett, T. P., Bouws, E., Carlson, H., Cartwright, D. E., Enke, K., Ewing, J. A., Gienapp, H., Hasselmann, D. E., Kruseman, P., Meerburg, A., Muller, P., Olsbers, D. J., Richter, K., Sell, W., and Walden, H.: Measurements of wind-wave growth and swell decay during the joint North Sea wave project (JONSWAP), 1973. Retrieved from: https://repository.tudelft.nl/islandora/object/uuid:f204e188-13b9-49d8-a6dc-4fb7c20562fc?collection=research.

Hasselmann, S., Hasselmann, K., Allender, J. H., and Barnett, T. P.: Computations and Parameterizations of the Nonlinear Energy Transfer in a Gravity-Wave Specturm. Part II: Parameterizations of the Nonlinear Energy Transfer for Application in
650 Wave Models, Journal of Physical Oceanography, 15(11), 1378–1391, https://doi.org/10.1175/1520-0485(1985)015<1378:CAPOTN>2.0.CO;2, 1985.

Hersbach, H., and Bidlot, J.-R.: The relevance of ocean surface current in the ECMWF analysis and forecast system, Workshop on Ocean-Atmosphere Interactions, Reading, United Kingdom, European Centre for Medium-Range Weather Forecasts, (November), 61–73, 2008.

655 Janssen, P. The Interaction of Ocean Waves and Wind. In The Interaction of Ocean Waves and Wind, https://doi.org/10.1017/cbo9780511525018, 2004.

King, R. R., While, J., Martin, M. J., Lea, D. J., Lemieux-Dudon, B., Waters, J., and O'Dea, E.: Improving the initialisation of the Met Office operational shelf-seas model. Ocean Modelling, 130(August), 1–14, https://doi.org/10.1016/j.ocemod.2018.07.004, 2018.

660 Lewis, H. W., Castillo Sanchez, J. M., Arnold, A., Fallmann, J., Saulter, A., Graham, J., Bush, M., Siddorn, J., Palmer, T., Lock, A., Edwards, J., Bricheno, L., Martínez-de la Torre, A., and Clark, J.: The UKC3 regional coupled environmental prediction system, Geosci. Model Dev., 12, 2357–2400, https://doi.org/10.5194/gmd-12-2357-2019, 2019.

Li, J.-G.: Hybrid multi-grid parallelisation of WAVEWATCH III model on spherical multiple-cell grids, Journal of Parallel and Distributed Computing, 167, 187–198, https://doi.org/10.1016/j.jpdc.2022.05.002, 2022.

665 Li, J. G.: Global transport on a spherical multiple-cell grid. Monthly Weather Review, 139(5), 1536–1555, https://doi.org/10.1175/2010MWR3196.1, 2011.

Li, J. G.: Propagation of ocean surface waves on a spherical multiple-cell grid, Journal of Computational Physics, 231(24), 8262–8277, https://doi.org/10.1016/j.jcp.2012.08.007, 2012.

Li, J. G., and Saulter, A.: Unified global and regional wave model on a multi-resolution grid, Ocean Dynamics, 64(11), 1657–
670 1670, https://doi.org/10.1007/s10236-014-0774-x, 2014.

NOAA: WAVEWATCH III® Production Hindcast, Multigrid: Feb 2005 to May 2019, retrieved from https://polar.ncep.noaa.gov/waves/hindcasts/prod-multi_1.php, 2020.

Palmer, T., and Saulter, A.: Evaluating the effects of ocean current fields on a UK regional wave model, Met Office Research Technical Report No: 612, 2016. Retrieved from https://library.metoffice.gov.uk/Portal/Default/en-
675 GB/DownloadImageFile.ashx?objectId=407&ownerType=0&ownerId=212801 (last access: 26/11/2022).

Piolle, J. F., Dodet, G., and Ash, E.: LOPS and CCI_Sea_state Team CCI+ Phase 1: Sea State cci Product User Guide, LOPS and Cci Sea State Team, 2020.

Saulter, A., Bunney, C., Li, J.-G., and Palmer, T.: Process and resolution impacts on UK coastal wave predictions from operational global-regional wave models, 15th International Workshop on Wave Hindcasting and Forecasting and 6th Coastal Hazard Symposium, 2017. Retrieved from http://www.waveworkshop.org/15thWaves/Papers/K1_WHF_SaulterEtAl_UKCoastalWave_20170913.pdf

Saulter, A. N., Bunney, C., King, R. R., and Waters, J.: An Application of NEMOVAR for Regional Wave Model Data Assimilation, Frontiers in Marine Science, 7(October), 1–19, https://doi.org/10.3389/fmars.2020.579834, 2020a.

Saulter, A.: North West European Shelf Production Centre - Quality Information Document, 1–60, 2020b. Retrieved from https://catalogue.marine.copernicus.eu/documents/QUID/CMEMS-NWS-QUID-004-014.pdf (last access: 26/11/2022).

Saulter, Andy, Bunney, C., and Li, J.: Application of a refined grid global model for operational wave forecasting, Forecasting Met Office Research Technical Report No: 614, 46, https://doi.org/10.13140/RG.2.2.22242.17600, 2016.

Siddorn, J. R., Good, S. A., Harris, C. M., Lewis, H. W., Maksymczuk, J., Martin, M. J., and Saulter, A.: Research priorities in support of ocean monitoring and forecasting at the Met Office, Ocean Science, 12(1), 217–231, https://doi.org/10.5194/os-12-217-2016, 2016.

Tolman, H. L.: User manual and system documentation of WAVEWATCH III® version 4.18, 2014. Retrieved from http://polar.ncep.noaa.gov/waves/wavewatch/manual.v4.18.pdf

Tonani, M, Pequignet, C., King, R., Sykes, P., Mcconnell, N., and Siddorn, J.: North West European Shelf Production Centre NORTHWESTSHELF_ANALYSIS_FORECAST_PHYS_004_013 Issue: 1.1. 1–46, 2021.

Tonani, M., Sykes, P., King, R. R., McConnell, N., Péquignet, A.-C., O'Dea, E., Graham, J. A., Polton, J., and Siddorn, J.: The impact of a new high-resolution ocean model on the Met Office North-West European Shelf forecasting system, Ocean Sci., 15, 1133–1158, https://doi.org/10.5194/os-15-1133-2019, 2019.

Valckle, S., Craig, T., and Coquart, L.: OASIS3-MCT User Guide, Cerfacs, Technical Report TR/CMGC/15/38, 2015.

Valiente, N. G., Saulter, A., Edwards, J. M., Lewis, H. W., Sanchez, J. M. C., Bruciaferri, D., Bunney, C., and Siddorn, J.: The impact of wave model source terms and coupling strategies to rapidly developing waves across the north-west european shelf during extreme events, Journal of Marine Science and Engineering, 9(4), https://doi.org/10.3390/jmse9040403, 2021a.

Valiente, N. G., Saulter, A., and Lewis, H. W.: The effect of different levels of coupling in surface wind waves along the NWS during extreme events, Met Office Forecasting Research Technical Report No:642, 2021b. Retrieved from https://digital.nmla.metoffice.gov.uk/IO_054d5518-86af-4a24-903d-fafa0d6a2695/ (last access: 26/11/2022).

Walters, D., Baran, A. J., Boutle, I., Brooks, M., Earnshaw, P., Edwards, J., Furtado, K., Hill, P., Lock, A., Manners, J., Morcrette, C., Mulcahy, J., Sanchez, C., Smith, C., Stratton, R., Tennant, W., Tomassini, L., Van Weverberg, K., Vosper, S., Willett, M., Browse, J., Bushell, A., Carslaw, K., Dalvi, M., Essery, R., Gedney, N., Hardiman, S., Johnson, B., Johnson, C., Jones, A., Jones, C., Mann, G., Milton, S., Rumbold, H., Sellar, A., Ujiie, M., Whitall, M., Williams, K., and Zerroukat, M.: The Met Office Unified Model Global Atmosphere 7.0/7.1 and JULES Global Land 7.0 configurations, Geosci. Model Dev.,

710   12, 1909–1963, https://doi.org/10.5194/gmd-12-1909-2019, 2019.

Waters, J., Lea, D. J., Martin, M. J., Mirouze, I., Weaver, A., and While, J.: Implementing a variational data assimilation system in an operational 1/4degree global ocean model, Quarterly Journal of the Royal Meteorological Society, 141(687), 333–349. https://doi.org/10.1002/qj.2388, 2015.

Williams, K. D., Copsey, D., Blockley, E. W., Bodas-Salcedo, A., Calvert, D., Comer, R., Davis, P., Graham, T., Hewitt, H.
715   T., Hill, R., Hyder, P., Ineson, S., Johns, T. C., Keen, A. B., Lee, R. W., Megann, A., Milton, S. F., Rae, J. G. L., Roberts, M. J., Scaife, A. A., Schiemann, R., Storkey, D., thorpe, L., Watterson, I. G., Walters, D. N., West, A., Wood, R. A., Woollings, T., and Xavier, P. K.: The Met Office Global Coupled Model 3.0 and 3.1 (GC3.0 and GC3.1) Configurations, Journal of Advances in Modeling Earth Systems, 10(2), 357–380, https://doi.org/10.1002/2017MS001115, 2018.

Young, I. R., and Verhagen, L. A.: The growth of fetch limited waves in water of finite depth. Part 1. Total energy and peak
720   frequency, Coastal Engineering, 29, 47–78, 1996.

WAVEWATCH III Development Group (WW3DG): User manual and system documentation of WAVEWATCH III® version 6.07. Tech. Note 333, NOAA/NWS/NCEP/MMAB, College Park, MD, USA, 465 pp. +Appendices, 2019.

Zieger, S.; Babanin, A.V.; Rogers, W.E.; and Young, I.R.: Observation-based source terms in the third-generation wave model WAVEWATCH, Ocean Model, 96, 2–25, doi:10.1016/j.ocemod.2015.07.014, 2015.